

# **Bose-Einstein condensation of $^{39}\text{K}$ with tunable interactions**

**Sahand Eslami**

supervisor **Giovanni Modugno**

**Università degli Studi di Firenze**







## Contents

1 Introduction.....	7
2 Theory.....	13
2.1 Bose-Einstein Condensates.....	13
2.1.1 Where to find a Bose-Einstein Condensate?.....	16
2.2 Gross-Pitaevskii theory.....	17
2.2.1 Gross-Pitaevskii equation.....	18
2.2.2 The time-independent GPE.....	20
2.2.3 Thomas-Fermi limit.....	21
2.3 Interactions, how to take control of them using the Feshbach resonances.....	23
3 Experimental setup.....	27
3.1 Experiment design.....	29
3.2 Vacuum system.....	30
3.3 Laser cooling.....	32
3.3.1 Magneto Optical Traps.....	38
3.3.2 Dipolar trap.....	39
3.3.3 Evaporative cooling.....	40
3.3.4 Laser frequency locking.....	41
3.3.5 Laser light modulation and amplification.....	42
3.4 Absorption imaging.....	43
4 Cooling of 39K to BEC and tuning the interaction.....	45
4.1 Laser cooling apparatus for the 39K.....	45
4.2 2D MOT.....	48
4.3 3D MOT.....	49
4.4 Magnetic mule.....	54
4.4.1 Magnetic trap transfer.....	55
4.5 Radio frequency evaporative cooling process and the Ramsauer-Townsend minimum.....	57
4.6 Bose Einstein Condensation in an optical trap.....	58
4.7 Interaction control.....	65
5 Conclusions.....	71



# 1 Introduction

Since the first observation of Bose-Einstein condensation of dilute atomic gases in 1995 [1], lot of experimental and theoretical research have been carried on and it now appears evident that Bose-Einstein condensation and in general ultracold atoms, offer vast possibilities for the investigation of the quantum behaviour of nature.

A Bose-Einstein condensate is a macroscopic quantum phenomenon. It is possible to directly observe and manipulate its quantum wave-function; in addition to this, matter-wave constituents have interactions and the presence of these interactions enriches the properties of condensed many-body systems with fascinating phenomena such as superfluidity. Many experiments have grown evidence of the superfluidity through the observation of quantized vortices, or observation of matter-wave solitons that all are proofs of the fact that condensates exhibit a macroscopic phase. It is the presence of an interaction term in the wave equation describing the system that is responsible for the non-linear behaviour of matter-waves.

In the field of atom interferometry, the need for non interacting Bose-Einstein condensates arises. In fact, ideal BEC represents the analogous of an optical laser for what concerns monochromaticity and coherence properties. As the laser emission, Bose-Einstein condensation of an ideal gas results from the occupation of a single atomic state, thus providing a coherent source of atoms for experiments.

The suppression of the atom-atom interactions results in the elimination of the *interaction-induced decoherence*, a phenomenon that blurs the effect of quantum interference thus limiting the interferometer performances. Moreover, the micrometric size of the atomic

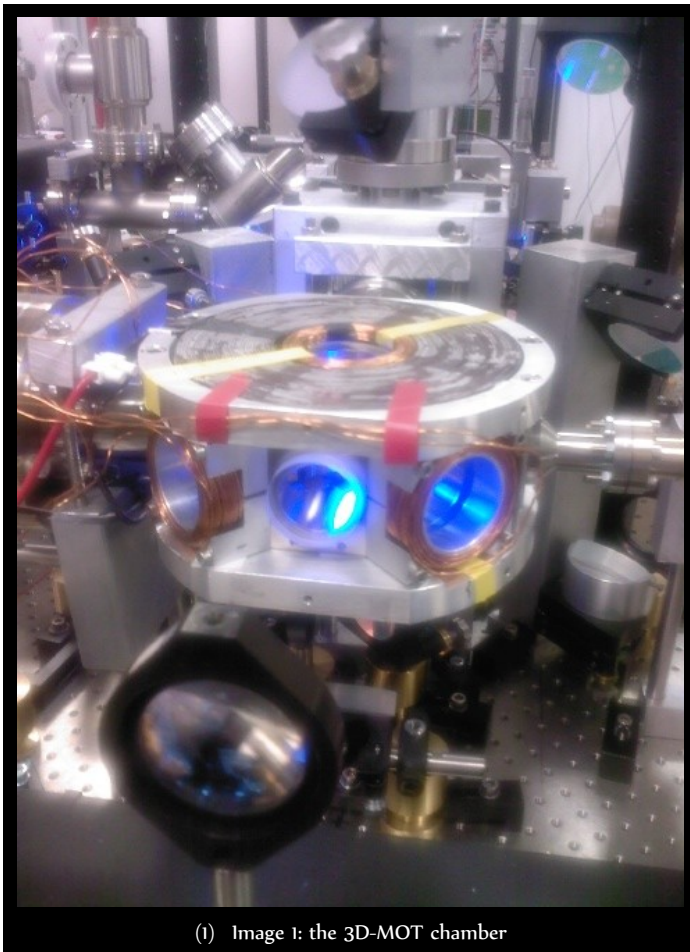
cloud of an ideal condensate makes this system very appealing for measurements with high spatial resolution. As far as atom interferometry is concerned, though, interaction may be extremely useful to prepare a wide variety of entangled states. These correlated states are very promising for the one achievable with non correlated particles. A system where interaction may be controlled is therefore very appealing for interferometric investigations. In contrast with the most many-body systems, where the interactions are imposed by the laws of nature, in quantum degenerate gases it is possible to gain control properly using the feature offered by the *magnetic Feshbach resonances*. In proximity of such resonances, the s-wave scattering length, shows a dispersive behaviour. This makes possible to *tune the interactions* virtually between  $+\infty$  and  $-\infty$  just varying the magnetic field around the resonance position.

Following the idea that was first introduced by Richard P. Feynman in the early '80s it is possible to use the tunability of this quantum degenerate gases to create some *Quantum Simulators*. In fact it is not actually possible to manage the complexity of most quantum systems, even with modern super-computers. With an appropriate choice of the interaction parameters, a quantum many-body system may simulate the behaviour of other quantum processes driven by the same Hamiltonian. We are in fact speaking of systems of ultracold gases overlapped by optical lattices, where the lattice potential is controlled in almost any characteristic: depth, periodicity, dimensionality or shape. Making use of Feshbach resonances also inter-atomic interactions can be modified. These systems offer the possibility to simulate and understand the physics of many condensed matter phenomena. Among these we find Bloch oscillations [2], the superfluid to Mott insulator phase transitions [3] or Anderson Localization [4].

The project in which I've worked during my thesis aims to the construction of a setup capable of realizing and control the Bose-Einstein condensate of  $^{39}\text{K}$ . This isotope was chosen due to its broad Feshbach resonance in the accessible magnetic field of a few hundred Gauss. This resonance allows a fine tunability of the interaction that ranges from strongly repulsive/attractive behaviour down to the ideal, non-interacting regime. So what we will obtain at last is a BEC with tunable interactions, which represents an ideal source of coherent matter-wave source. In order to obtain a BEC phase, it is necessary to implement tools for the

manipulation of matter-waves. Physicists have studied a variety of methods that could be implemented in our laboratory, and the most fascinating are the methods that exploit the forces resulting from the interaction between atoms and electromagnetic fields, in particular with laser sources. The “*Doppler cooling*” can be used from room temperature to approach the order of  $10^{-3} \text{ }^\circ\text{K}$  [5]. For some atomic species it is also possible to employ a “*Sub-Doppler cooling*” [6] which allows to reach the  $10^{-6} \text{ }^\circ\text{K}$  temperature range. Subsequent evaporation in a magnetic dipole trap is eventually used to go further down where usually BEC regime is achieved [1].

Various experiments with quantum gases are carried out with potassium atoms; both bosonic ( $^{39}\text{K}$ ,  $^{41}\text{K}$ ) and fermionic ( $^{40}\text{K}$ ) isotopes have been brought to the quantum degenerate regime [7] [8] [9]. In the fermionic case, quantum statistics along with the low energy of atoms in the system, imposes that low temperatures are attainable only if another



(1) Image 1: the 3D-MOT chamber

species is employed in the evaporative cooling stage (“*Sympathetic cooling*”). The peculiarity of potassium is that laser cooling and evaporative cooling are not very efficient. This characteristic led researchers to employ *sympathetic cooling* also for the bosonic isotopes.  $^{39}\text{K}$  and  $^{41}\text{K}$  have indeed been condensed using  $^{87}\text{Rb}$  as a coolant [7] [8]. The BEC realized with  $^{41}\text{K}$  alone ([10]) opened the way to single species condensation of bosonic potassium isotopes and straightforward to the construction of our apparatus, which is designed to overcome the ineffectiveness of cooling techniques and to realize a single species BEC of  $^{39}\text{K}$ . In the following we

briefly present and motivate the design and the main features of the laboratory in the department of physics at “Università degli Studi di Firenze”. We first realize a trap where we load atoms from a thermal gas and we virtually freeze two components of their velocity; this device is known as *2D-MOT* [11]. Here, the cooling and the confining processes take place only in two directions so that an atomic beam is created at the center of the trap. The atomic beam escapes from the *2D-MOT* chamber through a skimmer before being recaptured in a *3D-MOT*[12] placed in a *Ultra High Vacuum* environment.

This double trap system, along with large trapping volumes, ensures a very high loading rate for the *3D-MOT* where we achieve to capture more than  $10^9$  atoms in a few seconds. A large number of captured atoms in the *MOT* is necessary to counteract the low efficiency of the next cooling stages.

Afterwards the cooled  $^{39}\text{K}$  cloud is transferred from the *3D-MOT's* magnetic quadrupole trap to another analogous magnetic quadrupole trap mounted on a moving motorized ramp which moves the cloud to yet another chamber, which we will refer to as the *Science Chamber*. This is an orientable-mounting glass chamber, that supports the highest optical access, designed with the appropriate anti-reflection coating and capable to sustain the high pressure applied due to the difference of the vacuum pumped in the inside of  $\sim 10^{-12}$  bar. Another double-pair of independently controlled coils are mounted around this last chamber, one for trapping and another one for controlling the interactions of the atomic cloud. All the experiment is configured on electronic triggers and run with



(2) Image 2: view of the two tables where the experiment is being mounted

appositely created software in Matlab environment. The experiment is mounted on two anti-vibration tables, one completely dedicated to the control of the laser beams which when needed, through a series of optical fibres, is bring to the other table that hosts all the atomic vacuum chambers needed, the magneto-optical control systems and the imaging apparatus.



# 2 Theory

Let's introduce the theoretical concepts needed to understand the experiment.

First we will explain what is a **Bose-Einstein Condensate** and which is the mathematical model we use to understand the mechanics of such an object.

We then talk about the tool we use to tune the 2-body interactions of the condensate, the **Feshbach Resonances**.

## 2.1 Bose-Einstein Condensates

The theoretical prediction of Bose-Einstein condensation dates back more than 80 years. Following the work of Bose on the statistics of photons, Einstein considered a gas of non-interacting, massive bosons, and concluded that, below a certain temperature, a non-zero fraction of the total number of particles would occupy the lowest-energy single-particle state. In 1938 Fritz London suggested the connection between the superfluidity of liquid  $^4\text{He}$  and Bose-Einstein condensation. Superfluid liquid  $^4\text{He}$  is the prototype Bose-Einstein condensate, and it has played a unique role in the development of physical concepts. However, the interaction between helium atoms is strong, and this reduces the number of atoms in the zero-momentum state even at absolute zero. Consequently, it is difficult to measure directly the

occupancy of the zero-momentum state. It has been investigated experimentally by neutron scattering measurements of the structure factor at large momentum transfers, and the results are consistent with a relative occupation of the zero-momentum state of about 0.1 at saturated vapour pressure and about 0.05 near the melting pressure. The fact that interactions in liquid helium reduce dramatically the occupancy of the lowest single-particle state led to the search for weakly interacting Bose gases with a higher condensate fraction. The difficulty with most substances is that at low temperatures they do not remain gaseous, but form solids or, in the case of the helium isotopes, liquids, and the effects of interaction thus become large. In other examples atoms first combine to form molecules, which subsequently solidify.

The initial experiments were performed on vapours of rubidium, sodium, and lithium. So far, the atoms  $^1\text{H}$ ,  $^7\text{Li}$ ,  $^{23}\text{Na}$ ,  $^{39}\text{K}$ ,  $^{41}\text{K}$ ,  $^{52}\text{Cr}$ ,  $^{85}\text{Rb}$ ,  $^{87}\text{Rb}$ ,  $^{133}\text{Cs}$ ,  $^{170}\text{Yb}$ ,  $^{174}\text{Yb}$  and  $^4\text{He}^*$  (the helium atom in an excited state) have been demonstrated to undergo Bose–Einstein condensation. In related developments, atomic Fermi gases have been cooled to well below the degeneracy temperature and a superfluid state with correlated pairs of fermions has been observed. Also molecules consisting of pairs of fermionic atoms such as  $^6\text{Li}$  or  $^{40}\text{K}$  have been observed to undergo Bose–Einstein condensation. Atoms have been put into optical lattices, thereby allowing the study of many-body systems that are realizations of models used in condensed matter physics. Although the gases are very dilute, the atoms can be made to interact strongly, thus providing new challenges for the description of strongly correlated many-body systems. In a period of less than ten years the study of dilute quantum gases has changed from an esoteric topic to an integral part of contemporary physics, with strong ties to molecular, atomic, subatomic and condensed matter physics.

The dilute quantum gases differ from ordinary gases, liquids and solids in a number of ways, as I shall now illustrate by giving values of physical quantities. The particle density at the centre of a Bose–Einstein condensed atomic cloud is typically  $10^{13}\text{-}10^{15}\text{ cm}^{-3}$ . By contrast, the density of molecules in air at room temperature and atmospheric pressure is about  $10^{19}\text{ cm}^{-3}$ . In liquids and solids the density of atoms is of order  $10^{22}\text{ cm}^{-3}$ , while the density of nucleons in atomic nuclei is about  $10^{38}\text{ cm}^{-3}$ . To observe quantum phenomena in such low-density systems, the temperature must be of order  $10^{-5}\text{ K}$  or less. This may be contrasted with the temperatures at which quantum phenomena occur in solids and liquids. In solids,

quantum effects become strong for electrons in metals below the Fermi temperature, which is typically  $10^4$ – $10^5$  K, and for phonons below the Debye temperature, which is typically of order  $10^2$  K. For the helium liquids, the temperatures required for observing quantum phenomena are of order 1 K. Due to the much higher particle density in atomic nuclei, the corresponding degeneracy temperature is about  $10^{11}$  K.

The path that led in 1995 to the first realization of Bose–Einstein condensation in dilute gases exploited the powerful methods developed since the mid 1970s for cooling alkali metal atoms by using lasers. Since laser cooling alone did not produce sufficiently high densities and low temperatures for condensation, it was followed by an evaporative cooling stage, in which the more energetic atoms were removed from the trap, thereby cooling the remaining atoms.

Cold gas clouds have many advantages for investigations of quantum phenomena. In a weakly interacting Bose–Einstein condensate, essentially all atoms occupy the same quantum state, and the condensate may be described in terms of a mean-field theory similar to the Hartree–Fock theory for atoms. This is in marked contrast to liquid  $^4\text{He}$ , for which a mean-field approach is inapplicable due to the strong correlations induced by the interaction between the atoms. Although the gases are dilute, interactions play an important role as a consequence of the low temperatures, and they give rise to collective phenomena related to those observed in solids, quantum liquids, and nuclei. Experimentally the systems are attractive ones to work with, since they may be manipulated by the use of lasers and magnetic fields. In addition, interactions between atoms may be varied either by using different atomic species or, for species that have a Feshbach resonance, by changing the strength of an applied electromagnetic field. A further advantage is that, because of the low density, ‘microscopic’ length scales are so large that the structure of the condensate wave function may be investigated directly by optical means. Finally, these systems are ideal for studies of interference phenomena and atom optics.

### 2.1.1 Where to find a Bose-Einstein Condensate?

What we work on are gases, which, at room temperature, are well described by the Maxwell-Boltzmann statistics, which represents the probability  $p_n$  for the  $n$ -th atom in the gas to have an energy  $\epsilon_n$ , it asserts that

$$p_n \propto e^{\left(-\frac{\epsilon_n}{k_B T}\right)}.$$

It also is the high temperature limit for both the quantum statistical distributions:

$$\text{Fermi-Dirac:} \quad p_n \propto \frac{1}{e^{\frac{\epsilon_n - \epsilon_F}{k_B T}} + 1}$$

$$\text{Bose-Einstein:} \quad p_n \propto \frac{1}{e^{\frac{\epsilon_n - \epsilon_F}{k_B T}} - 1}$$

that describe respectively fermions (half spin particle ensembles) and bosons (integer spin particle ensembles).

The wave function for a system of identical bosons is symmetric under interchange of any two particles. Unlike fermions, which have half-odd-integer spin and antisymmetric wave functions, bosons may occupy the same single-particle state. An order of magnitude estimate of the transition temperature to the Bose–Einstein condensed state to the particle density, can be obtained comparing the thermal de Broglie wavelength, computed as the wavelength of the

free particle,  $\lambda_T = \sqrt{\frac{2\pi}{m k_B T}} \hbar$  with the mean interparticle spacing, which is of order  $n^{-1/3}$ .

Bose–Einstein condensation in an ideal gas sets in when the temperature is so low that  $\lambda_T$  is comparable to  $n^{-1/3}$ . For alkali atoms, the densities achieved range from  $10^{13} \text{ cm}^{-3}$  in early experiments to  $10^{15} \text{ cm}^{-3}$  in more recent ones, with transition temperatures in the range from 100 nK to a few  $\mu\text{K}$ .

From a theoretical point of view, much of the appeal of atomic gases comes out from the fact that at low energies the effective interaction between particles may be characterized by a single quantity, the scattering length. The gases are often dilute in the sense that the scattering length is much less than the interparticle spacing. This makes it possible to calculate the

properties of the system with high precision. For a uniform dilute gas the relevant theoretical framework was developed in the 1950s and 60s, but the presence of a confining potential gives rise to new features that are absent for uniform systems. The possibility of tuning the interatomic interaction by varying the magnitude of the external magnetic field makes it possible to study experimentally also the regime where the scattering length is comparable to or much larger than the interparticle spacing. Under these conditions the atomic clouds constitute strongly interacting many-body systems.[13]

Let's use some mathematics to better understand of what we are talking about. The behaviour of the condensed cloud of atoms is well described in the theory of Gross-Pitaevskii, which is the general mean field theory for the description of the many body interacting atoms system in the Bose-Einstein condensed state.

## 2.2 Gross-Pitaevskii theory

Let's consider  $N$  bosons with prevailing 2-body interactions in a dilute gas ( $na^3 \ll 1$ ),

where the interaction potential is  $\delta$ -like:

$$(1) \quad V(\vec{r}-\vec{r}') = g \delta(\vec{r}-\vec{r}') \quad \text{with} \quad g = \frac{4\pi\hbar^2 a}{m}$$

where  $a$  is the scattering length and  $m$  the mass of the bosonic atoms in the gas. In the field theory formulation, the Hamiltonian describing this system is:

$$(2) \quad \hat{H} = \int d\vec{r} \hat{\psi}^\dagger(\vec{r}) \left[ -\frac{\hbar^2}{2m} \nabla^2 + V(\vec{r}) \right] \hat{\psi}(\vec{r}) + \frac{g}{2} \int d\vec{r} \hat{\psi}^\dagger(\vec{r}) \hat{\psi}^\dagger(\vec{r}) \hat{\psi}(\vec{r}) \hat{\psi}(\vec{r}).$$

The time evolution of the field operator is given by the Heisenberg equation:

$$(3) \quad i\hbar \frac{\partial}{\partial t} \hat{\psi}(\vec{r}, t) = [\hat{\psi}(\vec{r}), \hat{H}]$$

the contribution of the kinetic and potential terms is:

$$(4) \quad \left[ -\frac{\hbar^2}{2m} \nabla^2 + V(\vec{r}) \right] \hat{\psi}(\vec{r})$$

but in the interaction part:

$$(5) \quad \begin{aligned} & \left[ \hat{\psi}(\vec{r}), \frac{g}{2} \int d\vec{r}' \hat{\psi}^{+2}(\vec{r}') \hat{\psi}^2(\vec{r}') \right] = \\ & = \frac{g}{2} \int d\vec{r}' [\hat{\psi}(\vec{r}), \hat{\psi}^{+2}(\vec{r}')] \hat{\psi}^2(\vec{r}') = \\ & = g \hat{\psi}^+(\vec{r}) \hat{\psi}^2(\vec{r}) \end{aligned}$$

substituting (4) and (5) in (3) we have:

$$(6) \quad i\hbar \frac{\partial}{\partial t} \hat{\psi}(\vec{r}, t) = \left[ -\frac{\hbar^2}{2m} \nabla^2 + V(\vec{r}) + g \hat{\psi}^+(\vec{r}, t) \hat{\psi}(\vec{r}, t) \right] \hat{\psi}(\vec{r}, t)$$

### 2.2.1 Gross-Pitaevskii equation

To find a semiclassical theory from the quantum fields written let's start defining,  $\phi = \langle \hat{\psi} \rangle$ . In general is possible to write

$$(7) \quad \hat{\psi} = \langle \hat{\psi} \rangle + \delta \hat{\psi}$$

where  $\delta \hat{\psi}$  represents the quantum fluctuations, but we are only interested in the ground state, such that in our case  $\langle \delta \hat{\psi} \rangle = 0$ .

The phase transition towards the Bose-Einstein condensate is associated with the

appearance of an order parameter different from zero. This parameter is the mean value of  $\hat{\psi}$ , which exactly represents the wave-function of the condensate. This is not an object that describes the individual particles but the collective environment of the system. The perturbing term is instead associated with the fraction of trapped atoms which are not condensed, and at very low temperatures their contribution is negligible.

By substituting  $\hat{\psi}(\vec{r}, t) \rightarrow \phi(\vec{r}, t)$  in (6) we get the Gross-Pitaevskii Equation (GPE):

$$(8) \quad i\hbar\phi(\vec{r}, t) = \left[ -\frac{\hbar^2}{2m}\nabla^2 + V(\vec{r}) + g|\phi(\vec{r}, t)|^2 \right] \phi(\vec{r}, t)$$

where the interaction constant  $g$  is related to the scattering length  $a$  by the relation

$$(9) \quad g = \frac{4\pi\hbar^2}{m}a$$

This is a non linear Schrödinger equation (with the non linear term linked to the inter-atomic interactions), and describes the time evolution of the wave-function of the condensate, related to the spatial density by

$$(10) \quad \rho(\vec{r}, t) = |\phi(\vec{r}, t)|^2$$

a quantity that is measurable in the experiment.

Now remember the definition of the number operator:

$$(11) \quad \hat{N} = \int d\vec{r} \hat{\psi}^\dagger(\vec{r})\hat{\psi}(\vec{r})$$

in the mean field approximation ( $\langle \delta\hat{\psi} \rangle = 0$ ) we have that

$$\begin{aligned}
(12) \quad \langle \hat{N} \rangle &= \int d\vec{r} \langle (\phi + \delta \hat{\psi})^\dagger (\phi + \delta \hat{\psi}) \rangle \\
&= \int d\vec{r} (|\phi|^2 + \langle \delta \hat{\psi}^\dagger \delta \hat{\psi} \rangle) \\
&\approx \int d\vec{r} \rho(\vec{r}, t) = N
\end{aligned}$$

so that the condensate's wave-function can be normalized substituting  $\phi \rightarrow \sqrt{N} \phi$ ; this in turn changes the interaction constant  $g \rightarrow Ng$ .

## 2.2.2 The time-independent GPE

Looking for the fundamental state of the system, one looks for solutions like:

$$(13) \quad \phi(\vec{r}, t) = \phi(\vec{r}) e^{-\frac{i\mu t}{\hbar}}$$

By substituting in (8) one obtains the time independent GPE:

$$(14) \quad \left[ -\frac{\hbar^2}{2m} \nabla^2 + V(\vec{r}) + g|\phi(\vec{r})|^2 \right] \phi(\vec{r}) = \mu \phi(\vec{r})$$

where  $\mu$  is the *chemical potential*, which is the energy needed for adding an atom to the system. This is different from the total energy of the system, in fact integrating

$$(15) \quad \int \phi^*(\vec{r}) \left[ -\frac{\hbar^2}{2m} \nabla^2 + V(\vec{r}) + g|\phi(\vec{r})|^2 \right] \phi(\vec{r}) d\vec{r} = \int \mu \phi(\vec{r}) d\vec{r}$$

results

$$\begin{aligned}
 & E_{\text{kin}} + E_{\text{pot}} + 2 E_{\text{int}} = \mu N \\
 (16) \quad & \mu = \frac{E_{\text{kin}} + E_{\text{pot}} + 2 E_{\text{int}}}{N} = \frac{E}{N} + \frac{E_{\text{int}}}{N}
 \end{aligned}$$

where  $E$  is the total energy of the system

$$(17) \quad E = E_{\text{kin}} + E_{\text{pot}} + E_{\text{int}}$$

if  $\epsilon = \frac{E}{N}$  is the energy for each particle, we can observe that

$$(18) \quad \mu = \epsilon + \epsilon_{\text{int}}$$

## 2.2.3 Thomas-Fermi limit

In the limit in which the interactions term is predominant with respect to the kinetic term, the time independent GPE could moreover be simplified, neglecting the latter:

$$(19) \quad H_{\text{Thomas Fermi}} = [V(\vec{r}) + g|\phi(\vec{r})|^2]$$

and then we can obtain the spatial distribution of the condensate. To be more explicit, we consider an external harmonic potential:

$$(20) \quad V(\vec{r}) = V_{ho}(\vec{r}) = \frac{1}{2} m \sum_i (\omega_i r_i)^2 = \frac{1}{2} m \omega_{ho}^2 r^2$$

where  $\omega_{ho} = \sqrt[3]{\omega_x \omega_y \omega_z}$  in the simplified spherical symmetry conditions.

We then obtain for the Gross-Pitaevskii equation in the Thomas-Fermi limit:

$$(21) \quad \begin{aligned} |\phi|^2 &= g^{-1}(\mu - V_{ho}(\vec{r})) = \\ &= \frac{\mu}{g} \left( 1 - \sum_i \frac{m \omega_i^2}{2\mu} r_i^2 \right) \end{aligned}$$

and defining  $R_i^{TF} = \sqrt{\frac{2\mu}{m \omega_i^2}}$  in the i-th direction:

$$(22) \quad |\phi|^2 = \frac{\mu}{g} \left( 1 - \sum_i \left( \frac{r_i}{R_i^{TF}} \right)^2 \right)$$

The chemical potential can be evaluated in the Thomas-Fermi limit from the normalization condition as shown here:

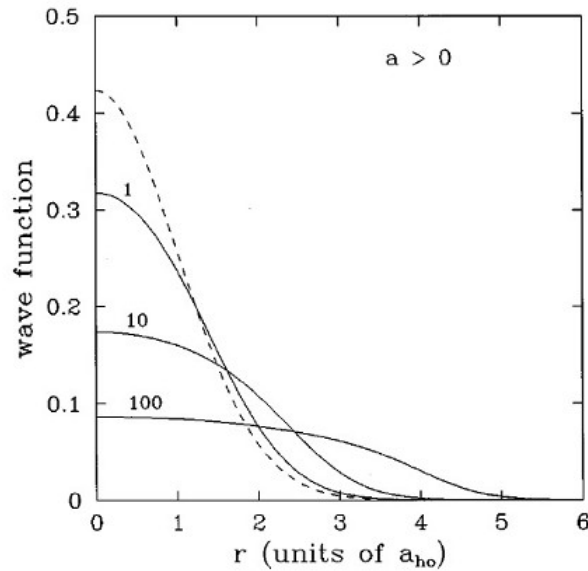
$$(23) \quad \begin{aligned} N &= \int d^3 r |\phi|^2 = \frac{\mu}{g} \int d^3 r \left( 1 - \sum_i \left( \frac{r_i}{R_i^{TF}} \right)^2 \right) = \\ &= \frac{\mu}{g} \prod_i R_i^{TF} \int d^3 \xi \left( 1 - \sum_i \xi_i^2 \right) = \\ &= \left( \frac{2\mu}{\hbar \omega_{ho}} \right) \frac{a_{ho}}{15 a} \\ &\quad , a_{ho} = \sqrt{\frac{\hbar}{m \omega_{ho}}} \end{aligned}$$

So we get for the chemical potential:

$$(24) \quad \mu = \frac{\hbar \omega_{ho}}{2} \left( 15 N \frac{a}{a_{ho}} \right)^{\frac{2}{5}} \propto N^{\frac{2}{5}}$$

We see in the next plot ( Image 3) the changing density profile of the condensate, from the dashed line which represents the perfectly non-interacting case ( $a=0$ ), where we find the

Gaussian distribution, to the Thomas-Fermi limit ( $a \gg 1$ ) where the interactions cause an enlargement on the profile, and it is now similar to a parabolic shape.



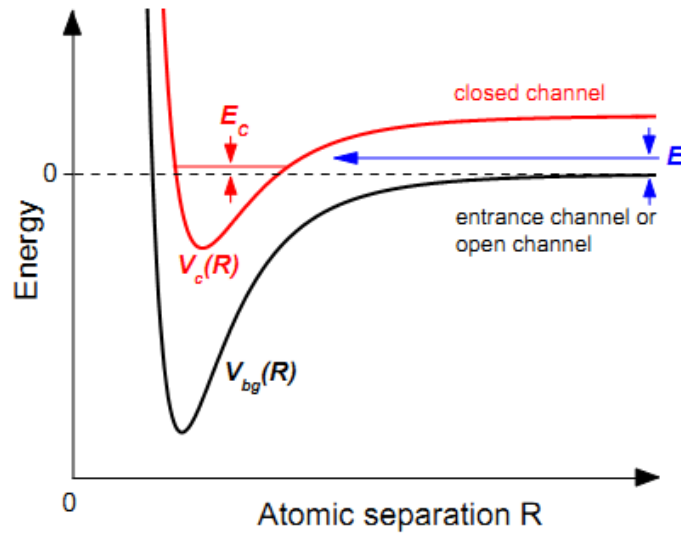
(3) Image 3: radial density distribution at different values of the scattering length  $a$

## 2.3 Interactions, how to take control of them using the Feshbach resonances

It is actually possible to take control of the interactions inside a quantum gas and be able to play with it. In practice one finds that this is achievable for most of the alkali gases. In fact, taking advantage of the Feshbach resonances [15], it is possible to alter the natural *s-wave scattering length*, which is the key parameter that regulates interactions in ultracold dilute gases. Looking at the formulas found in the previous section, this corresponds with the scattering parameter  $a$ .

Ultracold dilute gas of atoms normally interact via two body collisions at very low momentum. We will here present results derived in this limit so that we will give some details

about the behaviour of the s-wave scattering length.



- (4) Image 4: Basic two-channel model for a Feshbach resonance. The phenomenon occurs when two atoms colliding at energy  $E$  in the entrance channel resonantly couple to a molecular bound state with energy  $E_c$  supported by the closed channel potential. In the ultracold domain, collisions take place near zero-energy,  $E \rightarrow 0$ . Resonant coupling is then conveniently realized by magnetically tuning  $E_c$  near 0, if the magnetic moments of the closed and open channel differ.

The Hamiltonian of two colliding masses  $M_1$  and  $M_2$  is

$$(25) \quad H = \frac{p_1^2}{2M_1} + \frac{p_2^2}{2M_2} + V(\vec{r}_1 - \vec{r}_2)$$

which can be written conveniently in the center mass like

$$(26) \quad H = \frac{P^2}{2M} + \left[ \frac{p^2}{2\mu} + V(\vec{r}) \right]$$

where we have used  $\vec{P} = \vec{p}_1 + \vec{p}_2$  as the total momentum,  $\vec{p} = \vec{p}_1 - \vec{p}_2$  as the momentum

difference,  $\mu = \frac{M_1 M_2}{M_1 + M_2}$  as the reduced mass,  $\vec{r} = \vec{r}_1 - \vec{r}_2$  the relative coordinate, and

$M = M_1 + M_2$  as the total mass.

The bound and continuum states of the system properties are characterized finding the eigenstates of the system from the time independent equivalence:

$$(27) \quad \hat{H} \psi(\vec{r}) = E \psi(\vec{r})$$

where is  $\hat{H} = \frac{p^2}{2\mu} + V(\vec{r})$ .

We look for stationary solutions like:

$$(28) \quad \psi_{\vec{k}}(\vec{r}) \sim e^{i\vec{k}\cdot\vec{r}} + f(k, \hat{n}, \hat{n}') \frac{e^{i\vec{k}\cdot\vec{r}}}{r}$$

relative to  $E_k = \frac{\hbar^2 k^2}{2\mu}$ ,  $\hat{n} \equiv \frac{\vec{k}}{k}$ ,  $\hat{n}' \equiv \frac{\vec{r}}{r}$ . This is the sum of solutions of a free particle wave-vector  $\vec{k}$  and a diffusive wave-function with amplitude  $f(k, \hat{n}, \hat{n}')$ , the *scattering amplitude*, which can be related to the *differential* or *total scattering cross section* as

$$(29) \quad \frac{d\sigma}{d\Omega} = |f(k, \hat{n}, \hat{n}')|^2 \quad \sigma = \int d\Omega |f(k, \hat{n}, \hat{n}')|^2$$

We can also say that in case of a potential with central symmetry, the problem reduces to the solution of the radial wave-function  $u_{k,l,m}(r)$  where the indices  $\{k, l, m\}$  corresponding to momentum, angular momentum and orbital angular momentum projection along the quantization axis and the related Schrödinger equation becomes

$$(30) \quad u_{k,l,m}''(r) + \left[ k^2 - \frac{l(l+1)}{r^2} - \frac{2\mu V(r)}{\hbar^2} \right] u_{k,l,m} = 0$$

Note that there is a *centrifugal barrier* term that raises as  $l \neq 0$ , and we can write the cross-section as a sum of the series of the various angular momentum contributions:

$$(31) \quad \sigma(k) = \sum_{l=0}^{\infty} \sigma_l(k)$$

In very low energy limit, we have a vanishing  $k$  and the kinetic energies are lower than the centrifugal barriers. In the zero-momentum approximation, only s-wave scattering will take place.

Within the low energy regime, the cross section for identical bosons approaches a constant value that can be written in terms of the *s-wave scattering length*  $a$  :

$$(32) \quad \sigma_{l=0}(k) = 2 \cdot 4 \pi \cdot a^2 \quad , k \rightarrow 0$$

This scattering is crucial in the field of atomic gases, in fact in the dilute gas (this means  $\rho|a|^3 \ll 1$ ) we have shown before that the many body system depends only on the scattering length and nothing else in the interactions.

# 3 Experimental setup

The experimental setup is very complex, due to the need of performing various stages of laser and evaporative cooling, of keeping the atoms in a ultra-high vacuum environment, and of performing a sequence of delicate operations on the atomic samples on a very short timescale. The complexity of the setup requests a careful development and optimization of the various parts.

The principal aspects of this experiment I have found critical to control are:

- the vacuum system
- the laser system
- the electronic systems

When I started working on this experiment there had been about two years of work on it. The laser table was almost complete but it was not working properly as a whole. The most urgent problems were the bad fluctuations of the polarization of the laser beam through the transmission in the optical fibers and eventually, not rarely, loss of coupling with the laser beams. The atomic table was instead very partially completed, the laboratory was waiting the special designed glass cell were condensation and the most important part of the science experiments where thought to be realized.

This is a picture taken just before I started working in the laboratory showing what was looking like the mounted experimental apparatus:

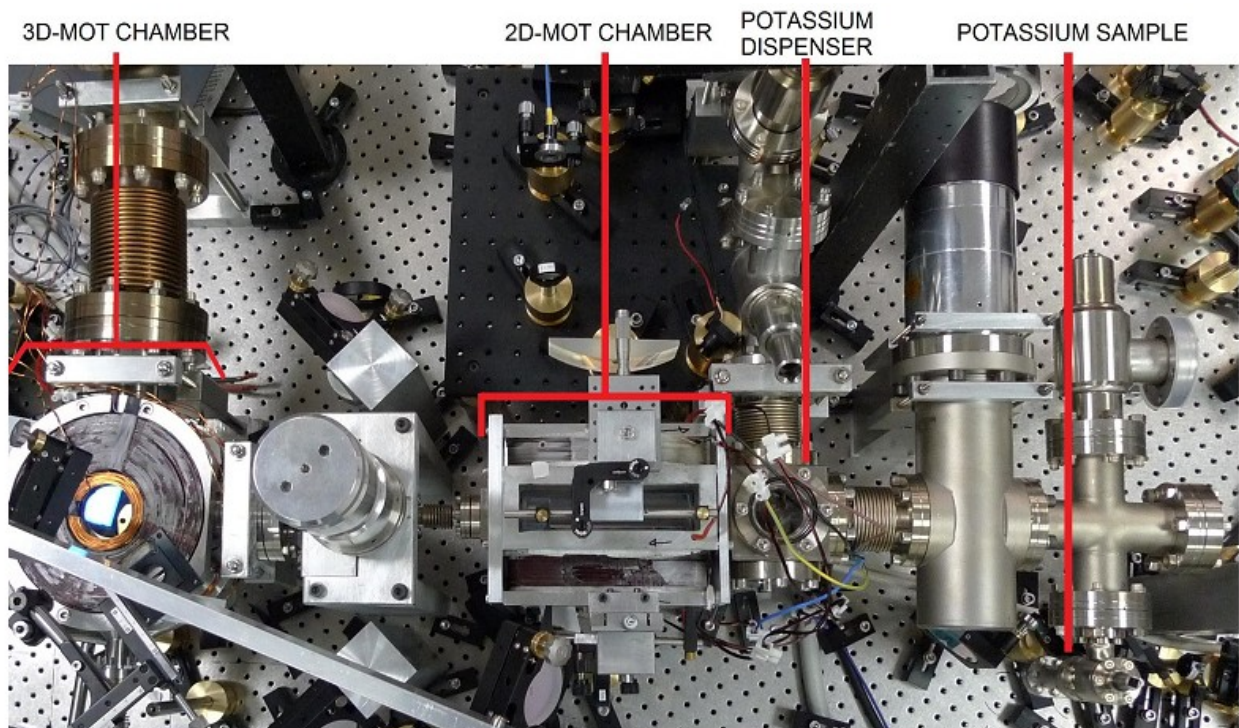
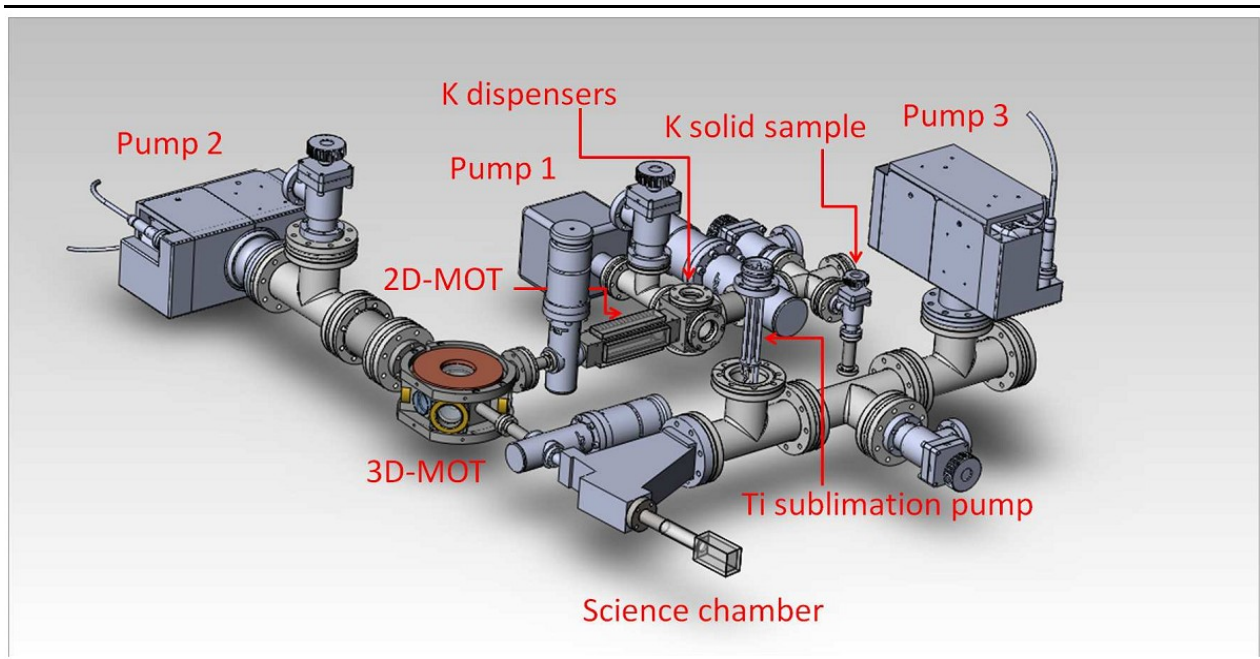


Image 5: Top view of the experiment when I did start working on it, with the pre-cooling 2D-Magneto Optical Trap and the 3D-Magneto Optical Trap

### 3.1 Experiment design

The system is designed to work with three main vacuum chambers. The first one is a 2 dimensional magneto-optical trap (2D-MOT) , which collects the background hot gas of potassium provided by the potassium dispenser cools the gas along the orthogonal directions and produces an atomic beam towards a second chamber (3D-MOT). Here the gas is loaded and sub-Doppler cooling is performed. Then the atoms are loaded in a magnetic trap mounted on a motorized stage which moves the atoms to a third chamber, called *science chamber* where once again the atoms are transferred in an optical dipole trap where evaporative cooling drops down the temperature towards Bose-Einstein condensation.



	2D-MOT	3D-MOT	Science Chamber
Pressure ( bar )	$10^{-11}$	$10^{-12}$	$10^{-14}$

## 3.2 Vacuum system

All the atomic chambers and pipes work under ultra-high vacuum conditions and this is one of the most difficult and critical part of the experimental work that needs care to be controlled. The processes of making and measuring this vacuum system was really interesting and on the technical aspect a whole new thing to me. I've learned the mounting and connection of the various vacuum control apparatus, pipes and atomic chambers and the use of vacuum and roughing pumps.

We have three molecular ionization pumps for the stabilization of the vacuum system in order to compensate for the out-gassing of the walls, positioned as far as possible from the various atomic chambers. First we used a turbo-molecular pump for a couple of weeks working continuously and monitoring with a series of gauge pressure sensors. As the pressure goes down you are able to have some data to compute a map of the pressure gradient through all the vacuum system and to figure out where are the leaks and figure out how to limit any of them. This is in particular the first objective of the whole process, as when you have chosen the pump you are going to operate (which has a specific pumping volume frequency at each working pressure), the better you are able to minimize the leaks, the lowest gets the limit vacuum pressure you are able to realize. The achievement of sufficiently low pressure values required a baking procedure that eliminates condensed water laying onto the internal surfaces of the system and most of the hydrogen accumulated in the steel during its fusion process. We baked all the steel components separately in an oven for approximately one day at 400°C to eliminate most of the hydrogen. After the system was assembled we baked the 2D-MOT and 3D-MOT parts at 120°C for five days. The chosen temperature was limited by the sealing glue used for the vacuum windows. The science chamber section was added later on and separately baked. Since there was no glue on this section, the baking temperature was chosen to be 200°C; again the procedure lasted for five days.

Also a Titanium Sublimation Pump was used to cover with a thin film of clean titanium the surrounding walls of the vacuum chamber. Since clean titanium is very reactive, components of the residual gas in the chamber which collide with the chamber wall are likely to react and to form a stable, solid product. Thus the gas pressure in the chamber is reduced.

The effectiveness of the TSP depends on a number of factors: the area of the titanium film, the temperature of the chamber walls and the composition of the residual gas, so e.g. the area is maximised considering where to mount the TSP.

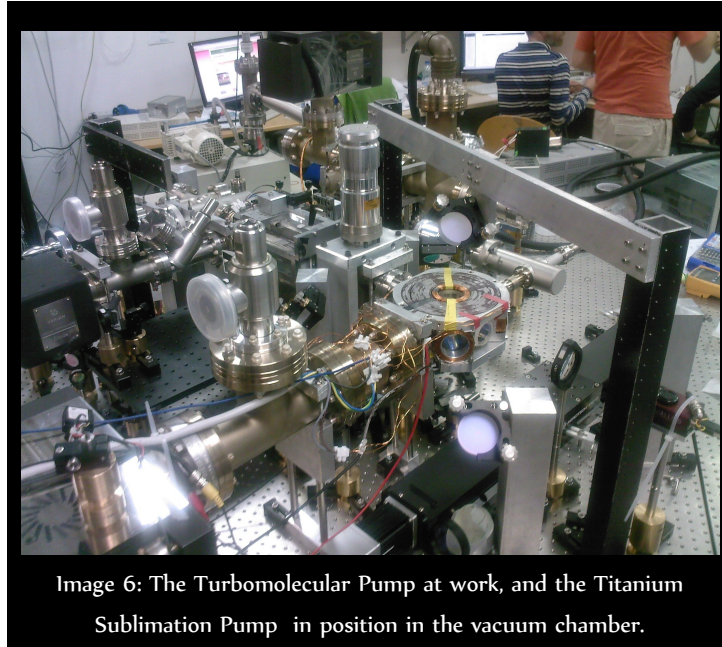


Image 6: The Turbomolecular Pump at work, and the Titanium Sublimation Pump in position in the vacuum chamber.

We are actually capable of stabilizing the vacuum system at an estimated pressure of  $10^{-14}$  bar in the last, large optical access, full glass atomic cell. We compute this using this relation:

$$(33) \quad P = \frac{L}{C}$$

where  $P$  is the vacuum pressure,  $L$  is the overall sum of leaks and out-gassing by the walls in the vacuum chamber,  $C$  is the gas conductivity of the various components ( $C_j$ ) also including the pumping volume the vacuum pumps ( $S_i$ ) computed as the inverse of the all the inverse conductivities like

$$(34) \quad \frac{1}{C} = \sum_i \frac{1}{S_i} + \sum_j \frac{1}{C_j}$$

### 3.3 Laser cooling

A cooling technique based on the collisions between the atoms in the gas and a cooled chamber walls is limited to temperatures that remains limited by the condensation temperature of the gas itself. With the cooling techniques shown in this section, it is however possible to reach temperatures below the millionth of a Kelvin. In fact, the coherence properties of the radiation emitted by a laser, makes it possible to consider it an ultra-cold system. The basic idea is in fact to cool atoms making them transfer energy to the electromagnetic field generated by the laser. In this way it is possible to trap and cool the atoms to obtain very low velocities, high densities and not to make them to collide with the chamber's walls. One obtains an ideal system for high resolution spectroscopy, collisional and atomic optics experiments.

For the principle of momentum conservation, an atom absorbing or emitting a photon will suffer a change in velocity called the recoil velocity  $v_r = \frac{h\nu}{mc}$  where  $h$  is the planck constant,  $\nu$  the photon's frequency,  $m$  the atomic mass and  $c$  the speed of light ( $h\nu/c$  is the momentum associated to the photon). For the D2 transition of  $^{39}\text{K}$  this results in  $v_r \sim 1.3 \frac{\text{cm}}{\text{s}}$ . After an absorption the atom has to decay again to the ground state in order to being able to absorb another photon. After the decay an atom emits a photon also but this happens in a random direction and the mean recoil effect due to emission is zero. Each cycle of absorption and decay can last a time of the order of the mean lifetime of the excited state

$\tau \sim 25 \text{ ns}$ . For an atom at room temperature ( $v_0 \sim 10^5 \frac{\text{cm}}{\text{s}}$ ) the number of photons to be

absorbed is of the order of  $N_{ph} = \frac{v_0}{v_r} \sim 10^5$ , this means that for stopping an atom will need few milliseconds. But to be more precise, the effective time for stopping an atom with laser light actually depends other than  $\tau$  on some other parameters, like the frequency and the

intensity of the radiation. Let's consider a model where an atom with just two quantum levels, a ground state  $E_g$  and an excited state, with energies  $E_g$  and  $E_e$  with a transition energy  $E_e - E_g = h\nu_A$  will interact with a plane wave radiation with frequency  $\nu_L$  and intensity  $I$  propagating in the direction  $\hat{n}$ . The difference  $\delta = \nu_L - \nu_A$  is called the detuning of the laser and we also define  $\Gamma = \frac{1}{2\pi\tau} = 6.2 \text{ MHz}$  to be the *natural broadening* of the atomic transition. The atom will suffer a mean radiation pressure force during the time interval of some absorption-decay cycles, given by[16]:

$$(35) \quad \vec{F}_{rp}(\vec{v}) = \hat{n} \frac{h\nu_L}{c} \frac{1}{2\tau} \frac{I/I_s}{1 + I/I_s + (4/\Gamma^2) [\delta - (\nu_L/c)\vec{v} \cdot \hat{n}]^2}$$

where  $I_s$  is called the saturation intensity and  $\delta_{eff} = \left[ \delta - \left( \frac{\nu_L}{c} \right) \vec{v} \cdot \hat{n} \right]$  represents the effective detuning between the laser frequency and the atomic transition frequency considering also the Doppler effect caused by the atom's movement. This makes sense if  $\delta_{eff}$  doesn't change much during this time.

Observe that this force has a maximum limit value  $F_{max} = h\nu_L / (2\tau c)$  for  $I \gg I_s$  which depends on the minimum time for an absorption-decay cycle. For a  $^{39}\text{K}$  atom this means that the maximum acceleration caused by the radiation pressure will be

$a_{max} = h\nu_L / (2m\tau c) \sim 3.4 \times 10^4 \text{ m/s}^2$  which is of the order  $10^3$  the gravitational acceleration in standard conditions.

There's also to say that there is a minimum temperature one could calculate to being able to reach with this cooling scheme for an atomic gas called the recoil temperature  $T_r$ . This limit is due to the fact that the energy and momentum exchange between the atoms and laser radiation happens by finite quantities, in fact this minimum temperature depends on the recoil momentum that one single photon can transfer:

$$(36) \quad \frac{1}{2} k_B T_r = \frac{1}{2m} \left( \frac{h v_L}{c} \right)^2$$

with  $k_B$  the Boltzmann constant. This is a very low temperature, of the order of the  $\mu K$ .

There's also another limit temperature called Doppler temperature  $T_D$ , which depends on the random spontaneous emission of photons in the atomic gas. For example, a group of atoms with a well defined momentum the spontaneous emission does not change the mean momentum value  $\langle p \rangle$  but will broaden the the indetermination on the values of momentum  $\langle p^2 \rangle$ . The Doppler temperature is

$$(37) \quad k_B T_D = \frac{h\Gamma}{2}.$$

which means  $T_D \sim 150 \mu K$ .

The use of laser radiation pressure force is implemented with two counter propagating beams on the same direction that invest the atoms. The laser is detuned lower than the atomic frequency so to use the Doppler shift to select in velocity the atoms and to interact mostly whit the atoms that are counter propagating against the laser beams. In fact, if the induced emission effect is negligible ( $I \ll I_s$ ), one can use the radiation exerted force shown in (35) for this configuration and obtain an overall force that is opposite to the velocity of each atom in the gas:

$$(38) \quad \vec{F}_{rp}(\vec{v}) = \hat{n} \frac{h v_L}{c} \frac{1}{2\tau} \left[ \frac{I/I_s}{1 + (4/\Gamma^2) [\delta - (v/c)v_L]^2} - \frac{I/I_s}{1 + (4/\Gamma^2) [\delta + (v/c)v_L]^2} \right]$$

for low velocities ( $v < \frac{\Gamma c}{2v_L}$ ) this force can be approximated to obtain

$$(39) \quad \vec{F}(\vec{v}) \sim h \left( \frac{v_L}{c} \right)^2 \frac{8\delta}{\Gamma} \left[ \frac{I/I_s}{[1+(2\delta/\Gamma)^2]^2} \right] \vec{v} = -\alpha \vec{v}$$

this is a viscous force and makes reason of way such a configuration is usually called an atomic molasse.

The achievable temperature in an atomic molasse is determined by two competing mechanisms: the first is the cooling by the viscous force just described, the second is a warming mechanism due to the discrete and stochastic momentum exchange between the atoms and the electromagnetic field. Depending on temperature of the cloud, one will be dominant. The equilibrium temperature will be where these mechanisms compensate each other. The cooling one of will cause a

$$(40) \quad \left( \frac{d \langle E_{\text{kin}} \rangle}{dt} \right)_{\text{cooling}} = F \vec{v} = -\alpha v^2 .$$

The warming mechanism, due to the spontaneous photon emission can be calculated using a one dimensional Brownian model. Consider to have an atom moving for example on the x axis, which can emit randomly emit a photon just on the +x or -x direction and

consequently suffering a recoil momentum depending on the frequency of the photon  $\frac{h\nu}{c}$  in the opposite direction. After N photon emissions, the mean value of the transferred momentum  $\langle p \rangle$  will be zero, but its variance  $\langle p^2 \rangle$  will be proportional to N:

$$(41) \quad \langle p^2 \rangle = N \left( \frac{h\nu}{c} \right)^2 .$$

So the warming mechanism modelized in this way will cause a

$$(42) \quad \left( \frac{d \langle E_{\text{kin}} \rangle}{dt} \right)_{\text{warming}} = \frac{1}{2m} \frac{d \langle p^2 \rangle}{dt} = 2 \frac{1}{2m} \frac{1}{2\tau} \frac{I/I_s}{1+(I/I_s)+(2\delta/\Gamma)^2}$$

where the doubling factor takes account also for the random adsorption direction.

The equilibrium temperature will be found when

$$(43) \quad \left( \frac{d \langle E_{\text{kin}} \rangle}{dt} \right)_{\text{warming}} + \left( \frac{d \langle E_{\text{kin}} \rangle}{dt} \right)_{\text{cooling}} = 0 .$$

Now using the definition of temperature

$$(44) \quad \frac{k_B T}{2} = M \frac{\langle v^2 \rangle}{2}$$

one can obtain

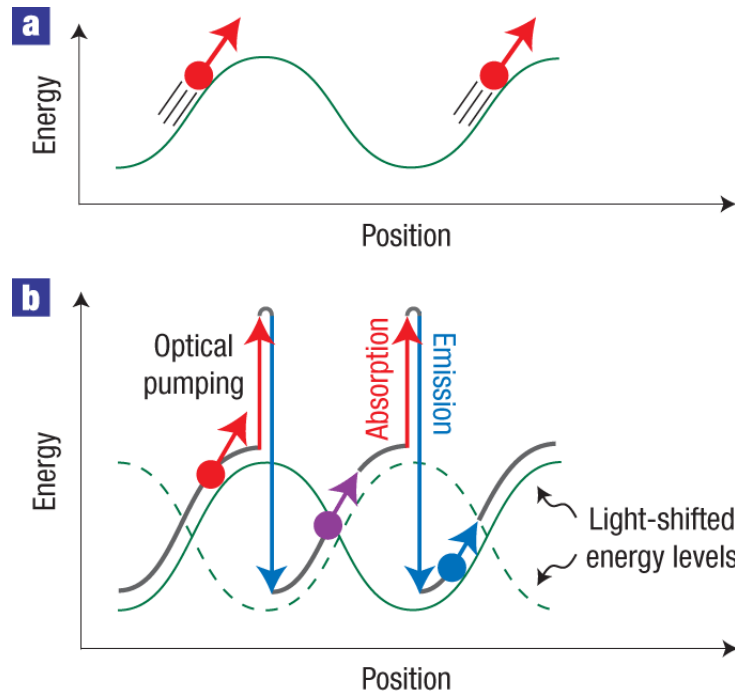
$$(45) \quad k_B T = \frac{h \Gamma}{4} \left( \frac{\Gamma}{2 \delta} + \frac{2 \delta}{\Gamma} \right) .$$

The minimum temperature of the molasse will be when  $\delta = -\Gamma/2$  . This is found to be the Doppler temperature  $k_B T_D = h \Gamma/2$  .

As we will see in the next chapter, it is actually possible to obtain much lower temperatures in the atomic molasse and will involve another cooling mechanism which is based on a cooling cycle called Sisyphus effect.

To understand how this effect works as a cooling mechanism, one has to consider the effect of the energy shift of the Zeeman levels involved in the cooling cycle, induced by a near resonance radiation. The shift depends on  $\frac{I}{\delta}$  and for a given Zeeman level it depends on the polarization of the radiation and the probability of the transition from the level itself. In particular, if the polarization of the radiation changes depending on the position, the shift will then depend on the position of the atom. If in an atomic molasse the two counter-propagating lasers have each a linear polarization along two orthogonal axes, the Zeeman levels will oscillate depending on the position under the effect of the light shift.

Now, to explain the cooling mechanism, let's consider the following figure [18]:



(a) An atom moving on a periodic potential converts potential into kinetic energy and vice versa, while keeping its total energy constant. After each period, the atom velocity, shown by the red arrow, remains constant.

(b) When the atom interacts with the two counter-propagating laser beams in the interference pattern produced by these lasers, the two ground-state energies (shown in green) of the atom vary sinusoidally with position. By choosing a suitable laser frequency, the atom can absorb an incoming photon, and make a transition (indicated by the red vertical arrows) to an excited state, but only at the top of the potential energy hills. The atom in the excited state can emit a photon (blue downward arrows), and then decay to the bottom of the valley. In the process, it loses an amount of energy equal to the energy difference between the absorbed and emitted photons, resulting in an energy loss leading to a successive slow-down after each cycle.

### 3.3.1 Magneto Optical Traps

The experiment starts with a 2D-MOT which cools the potassium gas from the dispenser on the orthogonal directions, resulting in a pre-cooled atomic beam which ignites the first 3D-MOT, in order to lower the loading time and allowing to start trapping cooler atoms. In general a MOT is a designed configuration of a inhomogeneous magnetic field (a quadrupole trap) and laser system analogous to an optical molasse, used to trap and cooling at the same time through laser radiation a gas of neutral atoms.

Let's consider the one dimensional scheme reported below (Image 7) and extrapolate each dimension implemented in the MOT as working independently. Consider to have two counter propagating laser beams with opposite circular polarizations  $\sigma_+$  and  $\sigma_-$  along the magnetic field direction for example along the  $\hat{x}$  axis, and an atom, for simplicity, with only 2 quantum states, the fundamental with

$J_f=0$  and the excited state with  $J_e=1$ . The magnetic field is zero in the center of coordinates and directed externally as you step out of the center, such geometry is realized with two counter propagating Helmholtz coils in order to obtain a magnetic quadrupole in the center of the trap. By Zeeman effect, the magnetic field shifts the sub atomic levels in function of the projection of the magnetic momentum along the direction of the field

$m_e = -1, 0, +1$ , as shown in figure. For the selection rule due to conservation of angular momentum  $J_x$

we obtain that the  $\sigma_-$  polarized beam coming from the right can only induce the transition to the  $m_e = -1$ , and the beam with  $\sigma_+$  polarized beam coming from the left side can excite just the transition to the  $m_e = +1$  state. If the laser beams have a detuning in frequency of  $\delta$  lower than the atomic transition, we have that an atom on the right side of the center of the trap will interact mainly with the beam from the right side causing a

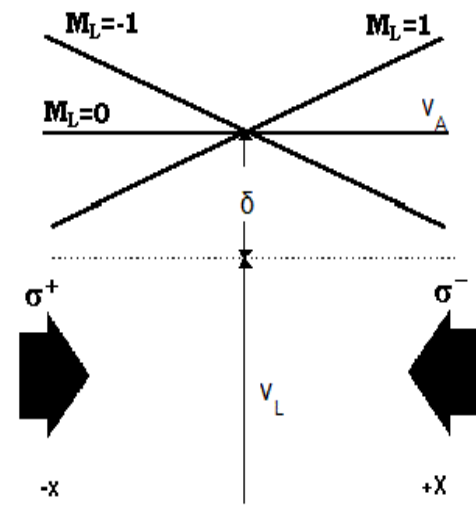


Image 7: scheme of MOT configuration

transition  $m_f=0 \rightarrow m_e=-1$ . In this way the overall effect of the radiation pressure on the atoms will be toward the center of the trap. The effect of the Magneto Optical Trap is that the atoms are not only confined but also cooled.

The loading rate of a MOT can be parametrized in this way:

$$(46) \quad \frac{dN}{dt} = R - \gamma N - \beta \int n^2 dV$$

where  $R$  is the *loading rate*,  $\gamma$  the *loss rate* due to collisions of the trapped with background free gas in the chamber and the last term gives the loss due to collisions of trapped atoms with density  $n$  and collisional coefficient  $\beta$ .

### 3.3.2 Dipolar trap

The dipolar trap is a pure optical trap. It is not caused by the radiation pressure but instead by dipole interaction proportional to the gradient of intensity of laser radiation. We can figure out how it works considering the atom as a forced harmonic oscillator. Its oscillating electric dipole  $\vec{d}$  is in phase with the electric field  $\vec{E}$  of the laser if the radiation frequency is less than the transition frequency, and in counter phase if it is higher. The interaction energy is  $W = -\vec{d} \cdot \vec{E}$ . For frequencies lower than the transition frequency,  $W$  is negative, and the atom is attracted towards regions of higher radiation intensity. In this way, by focusing a Gaussian radiation beam is possible to create a trap for the atoms around the maximum intensity position.

This kind of trap need to have the atoms already cooled because there's no dissipation of energy and hence no cooling effects. We use a high power laser in order to obtain a deep dipolar trap to minimize the losses in transferring the atoms from the transfer coils to the dipolar trap and to use evaporative cooling just lowering the intensity of the laser.

An other point is that in such a trap we find that the spontaneous emission of photons by

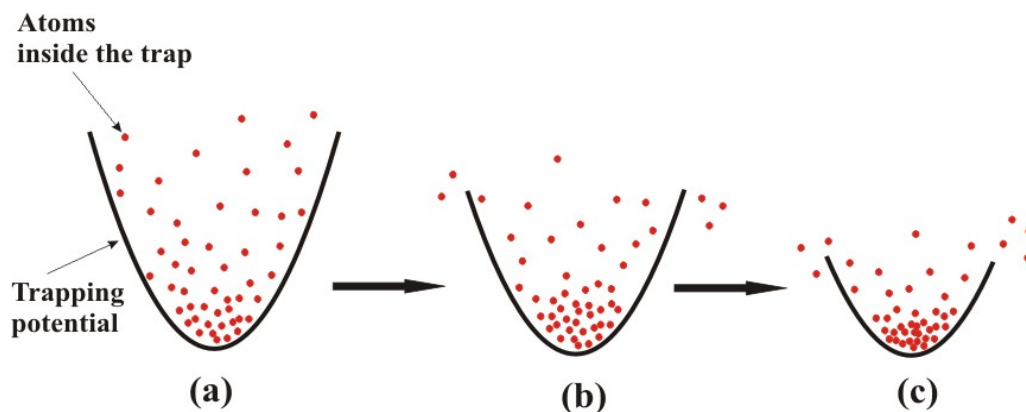
the trapped atoms, which will heat the cloud, is  $\propto \frac{I}{\delta^2}$ , where  $I$  the radiation intensity and  $\delta$  the detuning. So to achieve the longest trapping time is necessary to use the highest detuning possible, compatibly with the intensity of the laser.

The advantage of this trap, in our case, is when you need to have a system completely in the fundamental state without atoms hopping through levels in the cooling cycles.

### 3.3.3 Evaporative cooling

The evaporative cooling, is based on a selective loss of most energetic atoms and a successive rethermalization of the system. In fact, by losing only the most energetic atoms in the cloud one can lower the thermal energy of the whole system, lowering its temperature.

This kind of cooling had a key role in the achievement of the first Bose-Einstein Condensate as it is particularly effective to achieve high phase space densities and a large reduction in temperature.



We tried to implement this scheme of cooling by inducing spin-flip transitions with radio-frequency radiation using an antenna near the vacuum cell and a functional wave

generator, but the process could not be optimized for the potassium system probably for the low scattering length and hence a too much long thermalization time of the system. The evaporation cooling is achieved with a high intensity dipole trap which is progressively lowered by lowering the intensity of the laser radiation progressively in this way the deep of the dipole trap and letting by the way the hot atoms to escape.

### 3.3.4 Laser frequency locking

We need a frequency stabilization that is achieved by frequency modulation spectroscopy, a technique of saturation spectroscopy that provides a sub-Doppler frequency reference. It is realized with two counter propagating beams (known as pump and probe beams) on a glass containing potassium vapour sample. The intense pump beam depletes the population of the atomic ground states, producing a broad Doppler line in its spectrum. The weak probe beam absorption spectrum contains a broad line as well, but the spectrum has a narrow dip corresponding to atoms that are resonant with both beams, those with zero velocity. This is used as frequency reference.

In the modulation transfer scheme the pump beam is processed by a single passage electro optical modulation (EOM) stage. The EOM creates a 21 MHz oscillation on the beam phase. If the laser frequency is in the vicinity of an absorption line, the frequency modulation causes the saturation dip to modulate synchronously. In this way the frequency modulation on the laser has been converted into an amplitude modulation on the dip amplitude. The first derivative of this modulation has a zero crossing at the transition frequency. The signal is therefore processed and fed into proportional-integral (PI) controller. The PI elaborates the signal and drives the grating of the ECDL accordingly.

### 3.3.5 Laser light modulation and amplification

We lock the laser on the cooling transition ( $|F = 2\rangle \rightarrow |F = 3\rangle$ ). The repumping transition ( $|F = 1\rangle \rightarrow |F = 0, 1, 2\rangle$ ), is used to maintain the ground state of the cooling transition populated, it lies approximately 462MHz below it. All the 2D and the 3D-MOT require intense beams to saturate transitions involved in the trapping process.

Given that the saturation intensity ( $I_s$ ) is about 1.8 mW/cm<sup>2</sup> and that beam waists are of order 1 cm, an efficient trapping scheme requires a few hundred milliwatts coupled in the fibers. We achieve the required frequencies by stages in acousto-optic modulators (AOM) and we amplify those frequencies with master oscillator power amplifiers (MOPA) built in custom mount which implements a semiconductor tapered amplifier (TA).

We employ 3200-124 Crystal Technology modulators with 200MHz center frequency. The cooling light undergoes two double-passage stages in the AOMs, while the repumping light undergoes three double-passage stages to compensate for the 462 MHz splitting of the  $|F = 1\rangle \rightarrow |F = 2\rangle$  levels. This setup offers a frequency tunability over a few linewidths both for the cooling and the repumping light.

In order to obtain an amplification of laser radiation, Gallium Arsenide (GaAs) semiconductor tapered amplifiers (TA) produced by Eagleyard Photonics are placed onto a custom mount. A properly shaped seed beam of 40 mW is injected into the chip via a collimator. A current of 2.5 A is driven into the TA so that an output of up to 1.5W is obtained. We employ four TAs. Two of them are used to inject two double-passage stages of the light through the AOMs, and the other two are used to inject the 2D and the 3D-MOT beams. Before the double-passage in the AOMs, a mode-cleaning stage through optical fibers is required. All the above processes take place on a TMC 880 Series optical table. The transfer to the vacuum system table is realized through polarization maintaining NKT Photonics Crystal Fibers (LMA-PM-15) with KSI SMA-905 collimators. Before injecting the fibers, a single passage stage into a 80MHz AOM is performed. This last AOM achieves the amplitude control; it can also be used as a fast shutter.

The 2D-MOT fiber beam is split in four components with polarizing cube beam-splitters: two for the retro-reflected transverse beams, one for the plus beam and one for the push beam. Waveplates are placed to obtain the correct polarization of the light.

The 3D-MOT fiber beam is split with the same technique used for the 2D-MOT beam. We chose not to retro-reflect beams to avoid a shadow effect due to the absorption of the atoms and to compensate with less restrained beam paths for possible imperfections of the system. The six beams have a 18mm waist and 50mW power when they reach the cell.

### 3.4 Absorption imaging

This is performed by shining a laser on the atoms and by recording the image of the absorbed beam  $I_{out}(r)$  onto the CCD. A subsequent image is taken without atoms, the intensity in this case is indicated as  $I_{in}(r)$ . We infer the cloud density from the ratio of the two images via the Beer-Lambert law for the absorption. For this imaging system we always work with  $I/I_s \ll 1$ . In this case, the column density of the atomic cloud can be obtained as

$$(47) \quad n_{2D}(r) = -\frac{\ln\left(\frac{I_{in}(r)}{I_{out}(r)}\right)}{\sigma}$$

where  $\sigma$  is the scattering cross-section for the imaging light, can be written as

$$(48) \quad \sigma = \frac{3\lambda^2}{2\pi} \frac{1}{1 + \frac{4\delta^2}{\Gamma^2}}$$

the atomic parameters are then computed from the digital images by fitting the density distribution with this theoretical expression.



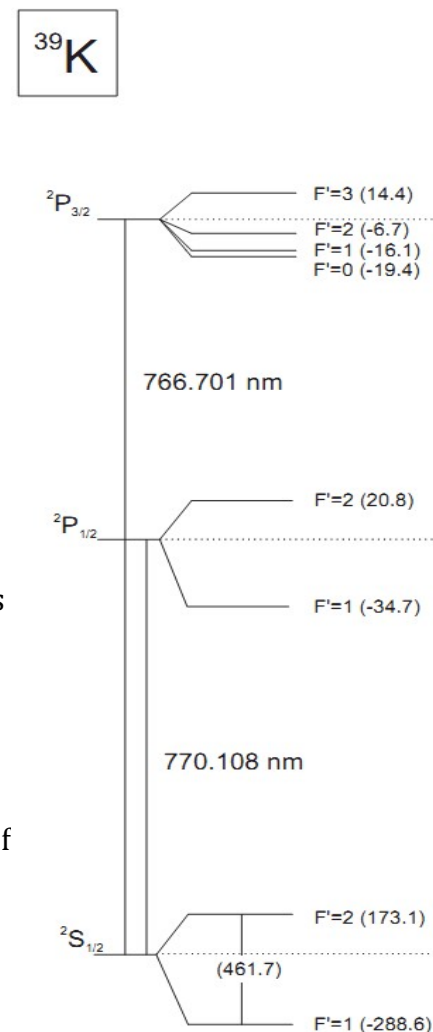
# 4 Cooling of $^{39}\text{K}$ to BEC and tuning the interaction

## 4.1 Laser cooling apparatus for the $^{39}\text{K}$

Alkali metals have a single valence electron more than the very stable configuration number of their previous noble element.

The fine structure interaction originates from the coupling of the orbital angular momentum  $\mathbf{L}$  of the valence electron and its spin  $\mathbf{S}$  with corresponding quantum numbers  $L$  and  $S$  respectively. The total electronic angular momentum is given by  $\mathbf{J}=\mathbf{L}+\mathbf{S}$  and the quantum number associated with the operator  $\mathbf{J}$  is in the range of  $|L-S| \leq J \leq L+S$ .

The hyperfine interaction originates from the coupling of the nuclear spin  $\mathbf{I}$  with the total electronic angular momentum  $\mathbf{F}=\mathbf{J}+\mathbf{I}$  where the quantum number  $F$  associated with the operator  $\mathbf{F}$  is in the range  $|J-I| \leq F \leq J+I$ , where  $I$  is the quantum number corresponding to the



operator  $\mathbf{I}$ .

Isotope	Atomic mass	Abundance(%)	Nuclear spin ( $I$ )	Magnetic moment ( $\mu/\mu_N$ )
$^{39}\text{K}$	38,9637074(12)	93,2581(44)	3 / 2	0,3914658
$^{40}\text{K}$	39,9639992(12)	0,0117(1)	4	-1,298099
$^{41}\text{K}$	40,9618254(12)	6,7302(44)	3 / 2	0.2148699

The Hamiltonian describing the hyperfine structure for the two excited states described above is given by

$$(49) \quad H^{hf} = \frac{a_{hf}}{\hbar^2} \mathbf{I} \cdot \mathbf{J} + \frac{b_{hf}}{\hbar^2} \frac{3(\mathbf{I} \cdot \mathbf{J})^2 + \frac{3}{2}(\mathbf{I} \cdot \mathbf{J}) - I^2 J^2}{2I(2I-1)J(2J-1)}$$

where  $a_{hf}$  and  $b_{hf}$  are the magnetic dipole and electric quadrupole constants respectively.

The dot product is given by  $\mathbf{I} \cdot \mathbf{J} = \frac{1}{2}(\mathbf{F}^2 - \mathbf{I}^2 - \mathbf{J}^2)$  and hyperfine interaction lifts the spin degeneracy due to the different values of the total angular momentum  $F$ . The energy shift of the manifolds are given by

$$(50) \quad \delta E_{hf} = \frac{a_{hf}}{2} [F(F+1) - I(I+1) - J(J+1)]$$

For a  $S = \frac{1}{2}$  system in the electronic ground state,  $J = \frac{1}{2}$ , the energy splitting due to the hyperfine interaction in zero field is given by

$$(51) \quad \Delta E_{hf} = \frac{a_{hf}}{2} \left( I + \frac{1}{2} \right)$$

In the presence of an external magnetic field the Zeeman interaction has to be taken into account:

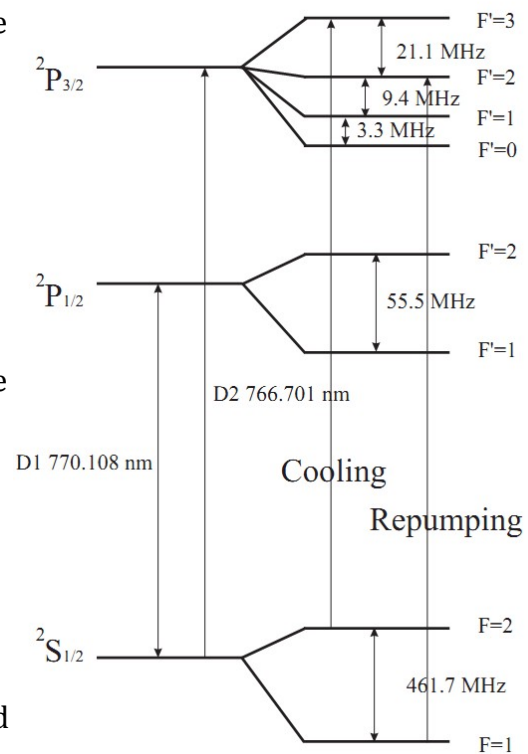
$$(52) \quad H^Z = \left( \frac{\mu_B}{\hbar} \right) (g_J \mathbf{J} - g_I \mathbf{I}) \cdot \mathbf{B}$$

where  $g_J$  is the Landé g-factor of the electron  $g_I$  the nuclear gyromagnetic factor.

$^{39}\text{K}$  has an electronic hyperfine two sub-level structure in the  $^2\text{S}_{1/2}$  ground state, corresponding to the total angular momentum eigenvalues  $F=\{1,2\}$ . In order to achieve best efficiency in the speed-dependent optical cooling mechanism we need to select the greatest interaction magnitude between radiation and atoms, therefore we consider the  $2 \rightarrow 3$  transition considering it's largest dipole moment. Unfortunately K has a strong out of resonance probability due to the narrow hyperfine splittings of the excited level, and this means that after short time, a single frequency cooling radiation will pump all the occupied levels to accumulate in the uncoupled ground state. So we use a bichromatic laser with a second frequency tuned to the  $1 \rightarrow 2$  transition. Both the Cooling ( $2 \rightarrow 3$ ) and Repumping ( $1 \rightarrow 2$ ) frequencies overlapped in the same bichromatic laser beam in the pairing on the optical fibers and both high intensity and large beams are sought to obtain faster capture rate of MOTs and increase the number of atoms they can trap.

Toptica DL Pro laser is stable but provides just 50 mW. It is successively amplified by 4 MOPAs, where the resulting amplified beam is precisely driven from the master laser spectrum but is emitted with fuzzy spatial modes, but optical fibers provide also spatial mode filtering. In the intermediate stage of amplification in the MOPAs we get a control on the different frequencies of the laser beams by the use of double paired 200MHz Acousto-optical modulators (AOM), and when needed, provide also a fast shutter action ( $\sim 3\mu\text{s}$ ) of the laser beam when needed. Mechanical shutters are also used, but are much slower ( $\sim 10^2\mu\text{s}$ ).

The 2D-MOT and the 3D-MOT chambers have each one a dedicated NKT PM-15 photonic crystal fiber. The MOPA coupling into the fiber has an efficiency of 50% so half of the power will be lost in this way. For the polarization we have a large 10% fluctuation, it needs periodic revision. The spectrum of the light out of the fibres is monitored through the use of a Fabry-Peròt resonator cavity.



We have the cooling and repumping components of the radiation with a difference in frequency equivalent to the hyperfine ground state splitting for the valence electron  $\Delta$ . Additional sidebands are present at  $\nu_R + \Delta$  and  $\nu_C - \Delta$ , with  $C$  stands for *cooling* and  $R$  stands for *repumping*, which are generated by non-linear effects inside the gain medium of the MOPA amplifier. However these sidebands are far detuned ( $\sim 400 \text{ MHz}$ ) with respect to the atomic transitions, such that their effect can normally be neglected.

## 4.2 2D MOT

Since the size of the laser beams at the output of the fibers is too small to provide a sufficiently large capture volume in the MOT, a proper telescope had to be realized. In particular, we use a double telescope, consisting in a first one with cylindrical symmetry, which provides beams of a radius of approximately 1cm, followed by a second one, where two cylindrical lenses enlarge one of the two spatial sizes to about 5cm. The laser is retro-reflected on the cell by two total internal reflections on two triangular base optical prisms. In this way we also maintain through double reflection the same helicity of the laser radiation.

On the long axis of the 2D-MOT we use two other beams one used as the 'push' beam and the other counter-propagating by reflection from below in vertical on a  $45^\circ$  gold coated reflective surface and anti deposition  $\text{MgF}_2$  coated mirror inside the vacuum chamber. This mirror has a 1.5mm diameter hole at the center where from the trapped atoms we 'push' in the next 3D-MOT chamber a 2D-cooled atomic beam.

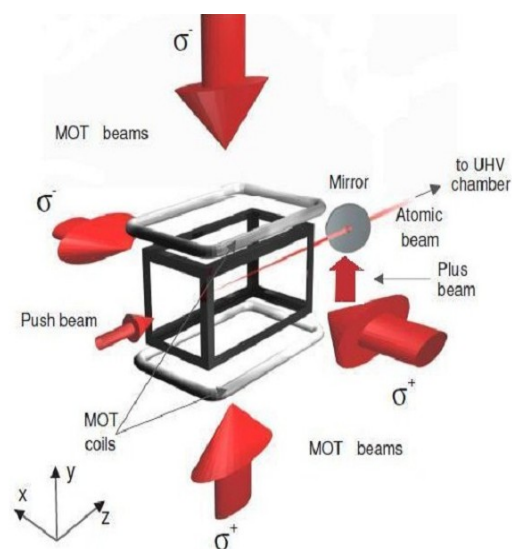


Image 8: 2D-Magneto Optical Trap Scheme

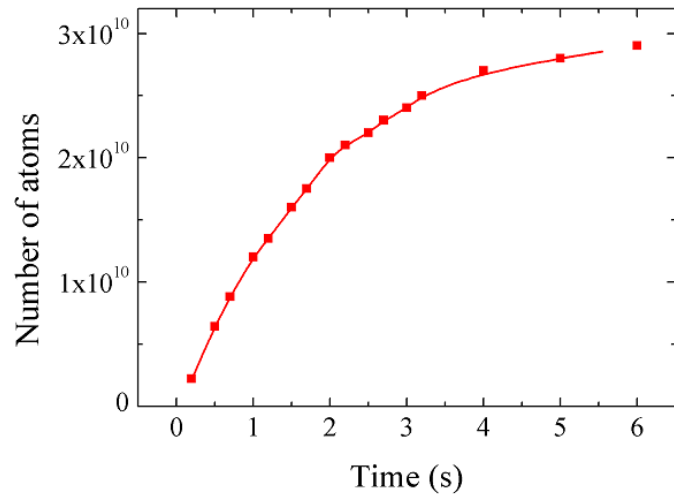
### 4.3 3D MOT

The 6 independent beams we use on the 3D-MOT are splitted by a single bichromatic beam of cooling and repumping from an optical fibre beam of 0.7mm waist. Each beam is circularly polarized through use of waveplates and magnified by a series of telescopes to obtain a waist of 17.5mm. The atomic cloud can be captured in all the volume occupied by all the crossing beams. As inflated by photon re-scattering, the atoms experience repulsive forces in between and they show a limitation in achievable density. This atomic cell is provided with 2 anti-Helmholtz coils capable to produce a gradient for the on axis magnetic field of

$$\frac{d\gamma}{dl} = 4.6 \frac{G}{cm \cdot A}$$

at an axial distance from the center of the trap 61mm, and other 3 pairs, each on the optical access windows of the chamber, these are 6 smaller ones used as 'compensation' coils, used to set the best offset of the center of the light trap and compensate the action of planetary magnetic field or other near machines disturbance.

This 3D-MOT starts trapping of the pre-cooled atomic beam that comes out from the 2D-MOT chamber on the action of the 'Push Beam': we observe a clear saturation in load capacity is reached just after 3s. Since the measured lifetime of the cloud in the cell is 4s, we deduce that this is due to background collisional losses.



These are the experimental parameters we used during the 3D-MOT loading:

	$\delta_C/\Gamma$	$\delta_R/\Gamma$	$I_{tot}/I_s$	$I_R/I_C$	$\gamma(G/cm)$
LOADING	-3	-3,3	35	0,8	11

We measured the atomic density of  $1.8 \cdot 10^{10}$  atoms/cm<sup>3</sup> and a temperature of 2mK. This

results in a phase space density of  $4.6 \cdot 10^{-9}$ . We have therefore to compress the MOT to raise the trapped number of atoms before starting the Sub-Doppler cooling process.

During the Compressed-MOT (C-MOT) we suppress the *repumping frequency* power and increase the detuning of the laser so that the light re-scattering effect is suppressed and the cloud gets compressed by the effect of the *cooling frequency*.

We suddenly change the MOT parameters for 5ms and then an adiabatic ramp of 10ms brings to these final values:

	$\delta_C/\Gamma$	$\delta_R/\Gamma$	$I_{tot}/I_s$	$I_R/I_C$	$\gamma(G/cm)$
initial	-3.7	$\pm 0$	35	0.5	15
adiabatic	-3.7 to -6.2	$\pm 0$	35	0.5 to 0.02	15

At this point the measures report  $1.8 \cdot 10^{10}$  atoms loaded in the trap, the density  $n$  is raised to  $1.7 \cdot 10^{11}$  atoms/cm<sup>3</sup> and the temperature is still 2mK. The phase space  $\rho$  is thus  $4.2 \cdot 10^{-8}$ .

Let's now discuss the main problems of cooling in presence of a narrow hyperfine splitting and a high density of the cloud. While in principle, the lowest achievable sub-Doppler temperatures are independent of the laser detuning  $\delta$ , the experiments with large density samples are performed at large detunings,  $\delta \gg \Gamma$ . This requirement arises from the need of keeping the scattering rate of photons by individual atoms low, in such a way that spontaneously emitted photons may not disturb the cooling process.

The way spontaneously emitted photons disturb the cooling is via re-scattering of them by other atoms. The optical thickness of the cloud

$$(53) \quad d = \sigma n l = \frac{3\lambda^2}{2\pi} \frac{I/I_s}{1 + I/I_s + 4\delta^2/\Gamma^2} n l$$

where  $\sigma$  is the scattering cross section and  $l$  is the average linear size of the cloud, represents the probability of absorption of a photon inside the cloud. When  $d$  becomes of the order of 1, or larger, the fluorescence photons emitted at the center of the cloud as a result of the cooling process itself, are likely to be reabsorbed on their way out. This causes many issues when working with dense samples ( $n > 10^9$  atoms/cm<sup>3</sup>). First of all, re-scattering generates an effective repulsive force which limits the achievable density. Moreover the reabsorbed photons effectively increase the diffusion coefficient in momentum space, causing the equilibrium temperature to increase. In principle, by increasing the detuning  $\delta$ , the thickness  $d$  can be reduced and the cooling becomes more efficient. However, most atomic systems cannot be modelled as simple two-level ones since they feature a hyperfine structure that is relevant for instance to Na, K and Rb. In this case, it is commonly thought that  $\delta$  must also be smaller than the main hyperfine splitting  $\Delta$ , since otherwise the presence of the other excited states would turn the sub-Doppler mechanism into a heating one. A problem therefore arises when trying to cool a dense sample in presence of a narrow hyperfine structure, since the increase of  $\delta$  needed to reduce re-scattering is limited by the hyperfine splitting. As a matter of fact, in the case of the

bosonic K isotopes, where  $\Delta \approx 2 - 3\Gamma$ , a clear sub-Doppler cooling has not been experimentally observed so far. The interesting detunings are the ones for which the cooling force is opposite to the atomic velocity. These are located either very close to resonance, where heating from photon re-absorption might be large, or for  $\delta \gg \Delta$ , where however the velocity capture range of the process becomes very low due to the large detuning. The conclusion one might draw is that efficient cooling

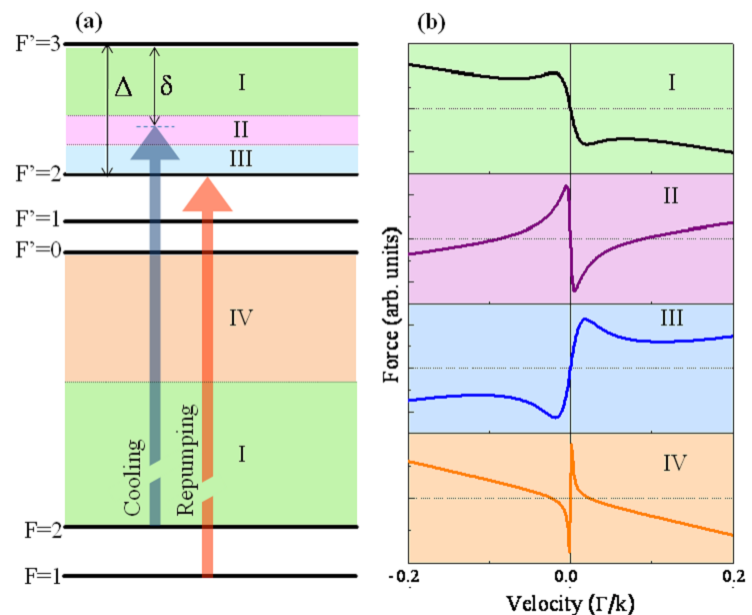


Image 9: a) shows the D2 hyperfine frequencies interval and the detuning of the cooling frequencies and , the hyperfine excited levels separation. b) computed by M. Landini, the velocity dependence of the radiation force in different frequency detuning interval. Here we can see that the only intervals suitable for sub-Doppler cooling are I and II.

for high density in potassium is not achievable.

The suitable detuning range which for the particular atom are useful for Sub Doppler cooling and the frequencies interval we have used to set up is shown in Image 9. In most experiments the cooling is performed in zone *I*, but in the case of Potassium we are forced to work in zone *II*, in order to suppress light-assisted re-scattering. We start this process as we have showed from a temperature of 2mK, this is not good for a direct cooling in this zone because of the heating of the hotter atoms that can be determined by the force for large velocity. In this case a pre-cooling can allow to keep all the atoms inside the velocity region in which the force is opposite to velocity and achieve efficient cooling. This is the first ingredient of our cooling strategy and it consists of the application of a linear ramp on the cooling parameters. From an initial condition of low detuning (zone *I*) and high power, to favour Doppler pre-cooling, we go to a final optimized condition for sub-Doppler cooling, with  $\delta$  in zone *II* and low intensity.

The second ingredient is the application of a dark molasses scheme, in which the low repumping beam intensity causes the atoms to occupy preferentially the  $F=1$  ground state, with only a small fraction of them in the  $F=2$ . The  $F=1$  is a dark state for the cooling light and therefore atoms in this state cannot absorb the re-scattered cooling photons. This expedient allows to suppress heating from multiple scattering events. For high densities the repumping intensity has to be kept very low (on the order of  $0.01 \times I_s$ ) in order to achieve low temperatures. For low density, instead, the repumping power is not important. In potassium, thanks to the narrow hyperfine structure an effective depumping rate of the cooling transition is present. The realization of a dark molasses is therefore easier than in other systems. In atomic systems with large hyperfine splitting, the implementation of a dedicated depumping beam is necessary to operate the dark molasse.

The optical molasses sequence is the most critical in the cooling of the cloud, in order to achieve low temperatures. We have indeed verified that a field of about 1G prevents us to reach sub-Doppler temperatures. Another subtle point is the power balance of the beams which has to be optimized for this phase, since the nulled magnetic field does not provide any longer the trapping force. The cooling is done by adiabatically increasing the detuning from zone *I* to zone *II* of the sub-Doppler force and, at the same time, ramping down the intensity.

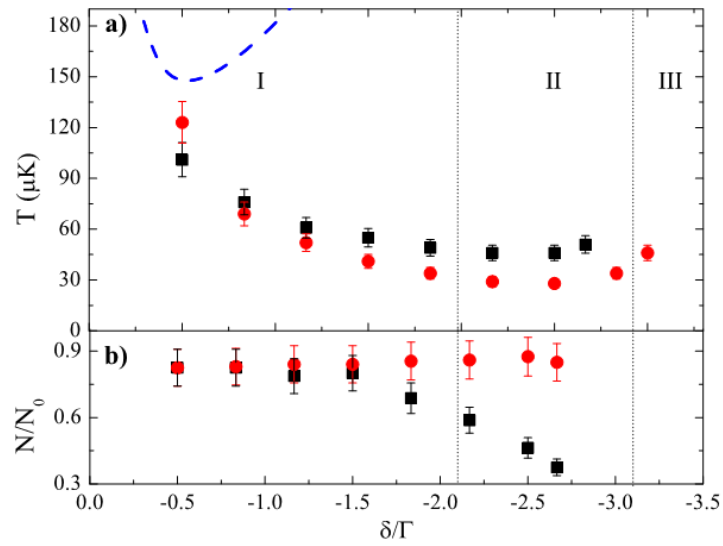


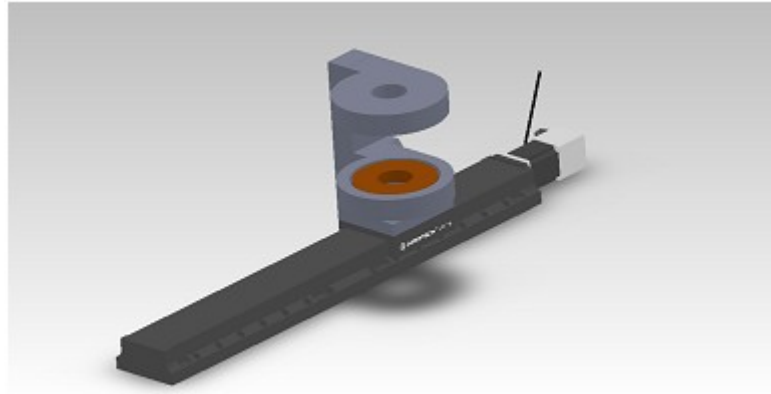
Image 10: in this graph are given the results during the ramp in the Sub-Doppler cooling, which is 10ms long (red squares), in comparison to the case without the ramp (black squares).

The following are the experimental parameters we actually use during these processes:

	$\delta_C/\Gamma$	$\delta_R/\Gamma$	$I_{tot}/I_s$	$I_R/I_C$	$\gamma(G/cm)$
Initial values	-0.7	-2.7	18	0.01	0
Adiabatic ramp	-0.7 to -2.5	-2.7	18 to 1	0.01	0

Without the adiabatic ramp, the cloud shows a bimodal distribution in relation to velocities. This is due to the characteristic of the II interval for frequencies defined before. The hotter tails are effectively accelerated by the cooling force.

## 4.4 Magnetic mule



Once cooled there has been designed a couple of coils mounted on a motorized moving support (Aerotech Pro115-600 linear stage) which can overlap on the 3D-MOT vacuum chamber. It entraps the atoms in the magnetic potential that is generated in its center and move the atomic cloud to the next atomic chamber: the '*science chamber*'. This transfer operation has been finely optimized in order to reduce losses or heating of the atoms in trap. This means that it gets accelerated of  $800 \text{ mm/s}^2$  to the speed of  $260 \text{ mm/s}$  and is then decelerated. All this movement takes  $2.4 \text{ s}$  moving the atomic cloud by  $540 \text{ mm}$ .

The transferring of the atoms from the 3D-MOT to the transport trap ( $200 \text{ ms}$ ) and the successive transfer to the trap which is built for the *science chamber* ( $500 \text{ ms}$ ), is done by ramping the current in the coils in order to minimize losses and heating.

In the next graph, we report a characterization of the movement of the cloud in the vacuued pipes that connect the *3D-MOT chamber* to the *science chamber*:

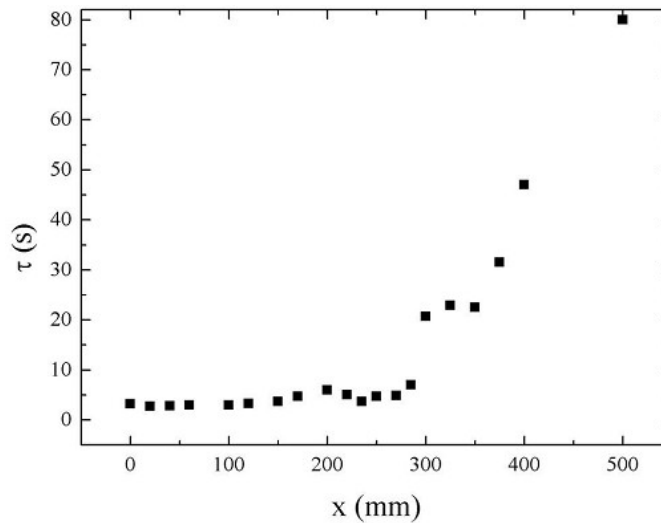


Image II: characterization of the movement of the cloud on the motorized ramp: the mean lifetime of the cooled cloud was measured moving the trapped atoms to the marked distances and back to the 3D-MOT where the atoms still in the trap where measured

#### 4.4.1 Magnetic trap transfer

To transfer atoms to the *transport coil's* trap we turn on the current in the coils at a specific current in order to be able to not heat up the atoms with a high potential gradient  $\gamma$ , and try too trap the highest number of atoms and not to lose them during the movement. For example, it's clear that the trap will have to compensate the weight of the atoms, and this means that  $\gamma > \gamma_{min} = 11.4 \text{ G/cm}$ . In the center of the trap there is a magnetic quadrupole gradient and we expect to being able to trap in this way just the atoms that experience an attractive potential (which is then linearly dependent from distance from the center), so as at the turn on most of the atoms will be in the  $F=1$  hence  $m_F = \{-1, 0, 1\}$ , it will be possible only to capture 1/3 of them. We transfer in the magnetic trap  $3.8 \times 10^9$  atoms,  $55 \mu\text{K}$ , at a density  $n = 1.8 \times 10^{11} \text{ atoms/cm}^3$  and phase space density  $\rho = 10^{-5}$ .

Once the atomic cloud is trapped, the magnetic field gradient is ramped up adiabatically to  $\gamma = 164 \text{ G/cm}$ . The sizes of the cloud shrinks by a factor 1.8 and its temperature is

increased by a factor 3.1, then the coils are moved toward the *science chamber*.

We tried to make some measurable characterization of the transport process. The dominant loss mechanism is due to background gas collisions, to estimate its effect we measured lifetimes  $\tau(x)$  of the sample at each point during the transport to the glass cell. To do so, we moved the cloud to the desired position, we kept it there for a variable time, and finally we moved it back to the MOT chamber, in which we measured the remaining number of atoms in the trap. The lifetime in the MOT chamber is only 4 s. The lifetime in the science chamber, instead, can reach 80 s. The lifetime in the intermediate region remains of the order of a few seconds up to the science chamber's pumping region.

It is interesting to notice that the lifetime increases significantly at about 200 mm from the 3D-MOT chamber and then lowers again. In this position, a vacuum valve determines a larger distance of the atomic sample from the apparatus walls. The increase in lifetime cannot be explained just by a lower background pressure, since the lifetime decreases in both directions towards the vacuum pumps, while it is reasonable that the pressure would decrease closer to the pumps. We do not have a clear explanation for this observation. The preparation of the cloud in the MOT chamber takes about 400 ms, in order for the compression ramp to be adiabatic. The losses during preparation are about 13%. By interpolating the measured lifetime and estimating the losses during the movement of the cloud as

$$(54) \quad \frac{\Delta N}{N} = \int_0^{t_f} \frac{dt}{\tau(x(t))}$$

we measure an overall additional loss of 32% moving cart. In total, the loss due to lifetime amounts to 41% of the initial atom number. The number of atoms measured in the last chamber is, however, only 21% of the initial atom number. An additional loss of about 50% can be explained by the cloud passing, somewhere during the transport, very close to an obstacle (one of the vacuum system's walls). Given the magnetic gradient in the trap and the temperature of the cloud, such a loss would be consistent with an obstacle at a distance of 1.5 mm from the center of the trap. Since the atoms lost by such an occurrence are the most

energetic ones, the atomic loss can determine cooling after thermalization of the cloud.

When the cloud reaches the glass cell of the *science chamber* the gradient is raised maximally to about 276 G/cm and on cloud measurements result  $N=8 \times 10^8$ ,  $T= 250 \mu K$ ,  $n=4 \times 10^{11}$  atoms/cm<sup>3</sup>,  $\rho = 2.3 \times 10^{-6}$ .

## 4.5 Radio frequency evaporative cooling process and the Ramsauer-Townsend minimum

When the cloud reaches the *science chamber*, we tried a radio-frequency evaporative cooling. This consists in inducing spin flip transitions that change the magnetic dipole projection of the atoms against the magnetic trap field and moving them in a Zeeman level in which they can no more be trapped. We however saw it was not work properly. In fact, trying to minimize the phase space density, by actioning a linear frequency ramp the high energy tail of thermal distribution, we didn't succeed in lowering effectively the temperature of the cloud.

This failure of the evaporative cooling can be attributed to a lack of rethermalization.

One can observe that the approximation in (32) is no longer valid for relatively high energies, since the higher level terms in (31) can't be any more neglected. This graph aside (Image 12), reports the numerical computation of A. Simoni (University of Rennes) of the scattering cross-section of two atoms in the  $|2, +2\rangle$  state against the collisional energy, in center of mass reference. It shows indeed a broad minimum in the scattering in correspondence of  $400\mu K$ , which is of the order of the energy in the tails of our distribution. This minimum is analogous to the Ramsauer-Townsend minimum studied in electronic

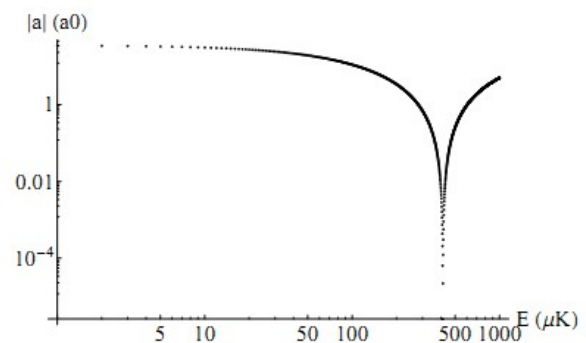


Image 12: log scale graphic showing the RT minimum in the  $|1,1\rangle$  state for the 2-body scattering length

scattering processes. To continue the evaporative cooling the atoms have therefore to be transferred to an optical trap.

## 4.6 Bose Einstein Condensation in an optical trap

Two laser beams, the main dipole trap beam and the dimple beam, are used for optical trapping.

The main dipole trap beam is derived from a IPG photonics YLR-100-LP-AC ytterbium fiber laser. This laser can provide up to 100W of laser power at a central wavelength  $\lambda=1064$  nm, with an emission linewidth of 2nm. We typically operate this laser at a lower power, around 30W, because the wide emission linewidth tends to induce photo-association of pairs of atoms into excited molecular states, which results in losses. Since these processes depend in a highly non-linear way on the laser intensity, they can be substantially reduced by lowering the power from 100W to 30 W. The laser is coupled into an AOM for power control, sent to a

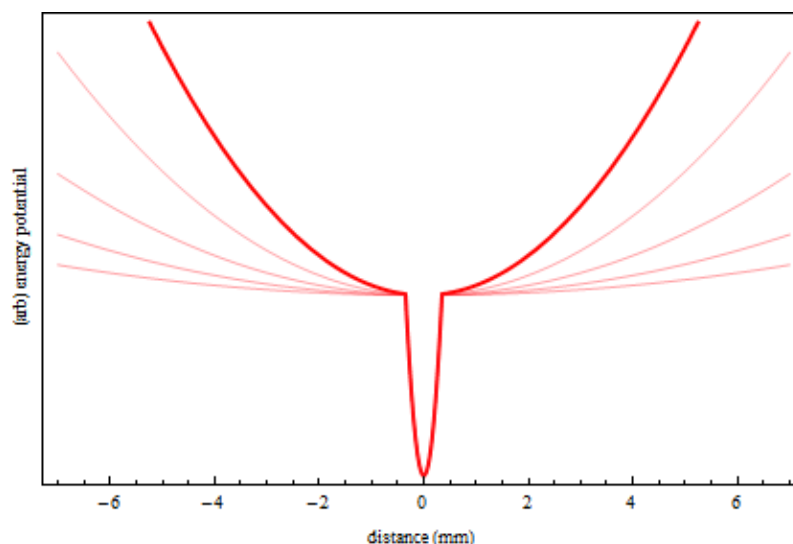


Image 13: energy potential at the center of the optical trap and graphical representation of the effect of ramping down the intensity of the IPG during the evaporation process

system of lenses and focused onto the atoms. The optics used for the beam preparation are made in fused-silica for its low absorption coefficient. On the last focusing lens we arrive with a 10mm waist. The last lens has a focal length of 300mm. The beam waist at the focus was measured to be  $25 \mu\text{m}$ , substantially larger than the  $10 \mu\text{m}$  Gaussian beam estimation. This is due to deterioration of the beam quality after the AOM and by spherical aberrations on the focusing lens. The use of a small waist is necessary in order to achieve three dimensional trapping with a single beam and to enhance the atomic collisional rate during the accumulation of the atoms in the trap. The use of a crossed dipole trap is not straight-forward for this laser because of the large spectrum. The laser's spectrum largely exceeds the hyperfine splitting of the ground state. For this reason, Raman transitions, in which a photon is absorbed from one beam and emitted into the other, are allowed and can lead to heating of the sample.

The dimple beam is generated by a Nufern Ytterbium fiber amplifier seeded by an Innolight Mephisto S S200 NE. The amplifier can provide up to 10W laser power. The optimized operation of the dimple trap requires only 200 mW. This beam, as the previous one, is sent to an AOM for power control, optically manipulated and focused onto the atoms. The laser waist at the atoms position is about  $70 \mu\text{m}$ . Due to its low trap depth, the dimple laser does not influence the atomic distribution before the last stages of evaporation. Its purpose is mainly to increase the trapping frequency, and consequently the collision rate, once the main dipole trap depth is too weak to sustain the evaporative cooling. The laser is however switched on at the beginning of the evaporation sequence and its power is kept constant.

Let us summarize the properties of the optical potential resulting from the combination of the two beams. The main dipole trap laser (horizontal) has a waist  $W_0=25 \mu\text{m}$  and its power is  $P=30\text{W}$ . Its depth is therefore 1.4 mK. The vertical dimple laser has a waist of  $70 \mu\text{m}$  and its power is 200 mW, giving additional 3.5  $\mu\text{K}$ . The truncation parameter is only determined by the main dipole trap along the horizontal direction, since the losses are mainly along gravity.

Collisions are crucial for the loading of the dipole trap. We decided to employ a very deep trap, in order for the mean energy of the atoms to increase once they fall inside the dipole. This, in turn, increases the collision rate and keeps the atomic energy higher than the

Ramsauer-Townsend minimum. We ramp up the dipole trap lasers to full power in 1s and we wait in the combined magnetic and dipole trap for additional 2 s, to give the time to the cloud to thermalize and accumulate in the deep dipole trap. We then switch off the quadrupole trap abruptly and collect the remaining atoms in the dipole trap. We do not perform neither RF evaporative cooling in the quadrupole nor adiabatic decompression of the trap, since the collision rate is too low in the magnetic trap to determine an efficient evaporation. We estimate a collision rate at the center of about 38 Hz but, due to the Ramsauer-Townsend minimum. The rate is indeed energy-dependent and reaches almost zero in the tails of the thermal distribution. Evaporative cooling requires redistribution of atoms at different energies in order to be efficient and is, therefore, affected by the lack of collisions at higher energies. The cloud parameters, just after switching off the magnetic field, are:  $N=1.4\times 10^7$ ,  $T=220\ \mu\text{K}$ ,  $n=5.1\times 10^{13}\ \text{atoms}/\text{cm}^3$  and  $\rho=1.4\times 10^{-4}$ . We ascribe the increase in phase space density to the dimple effect and to plain evaporation of the hot part of the cloud at the release of the magnetic trap.

After a calibration of the magnetic field on the atom position, using the most distant Helmholtz coils (*Feshbach coils*) around the *science chamber* we are able to use the Feshbach resonances reported in [14] to adjust the scattering length to positive values, where the RT minimum disappears, and therefore evaporation can proceed in a much more efficient way.

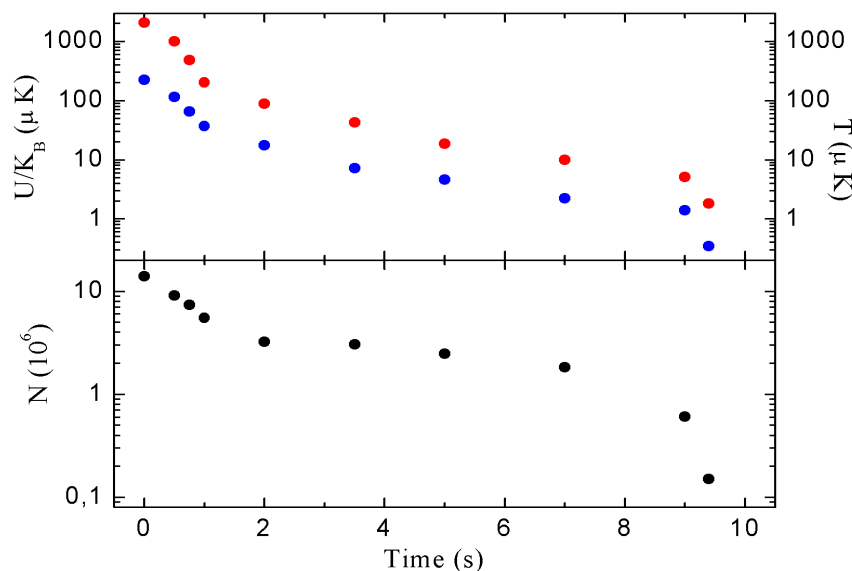


Image 14: evolution of the trap potential depth (U), temperature (T) and atom number (N) as a function of the evaporation time

When loaded in the optical trap the scattering length is suddenly changed to  $75 a_0$  and the power of the main beam is lowered to lose the external atoms from the dipole trap region and achieve evaporative cooling. The ramp is optimized on the time steps of a half-power lowering of the main beam in order to maximize the evaporation's efficiency.

Bose-Einstein Condensation is observed ( Image 15 ) when the phase space density of the system  $\rho = n \lambda_T^3$  is over  $\rho = 1$  . Below I report in the graph the measured phase space density during the same evaporation ramp, this shows that at the ending of the ramp this density is actually reached.

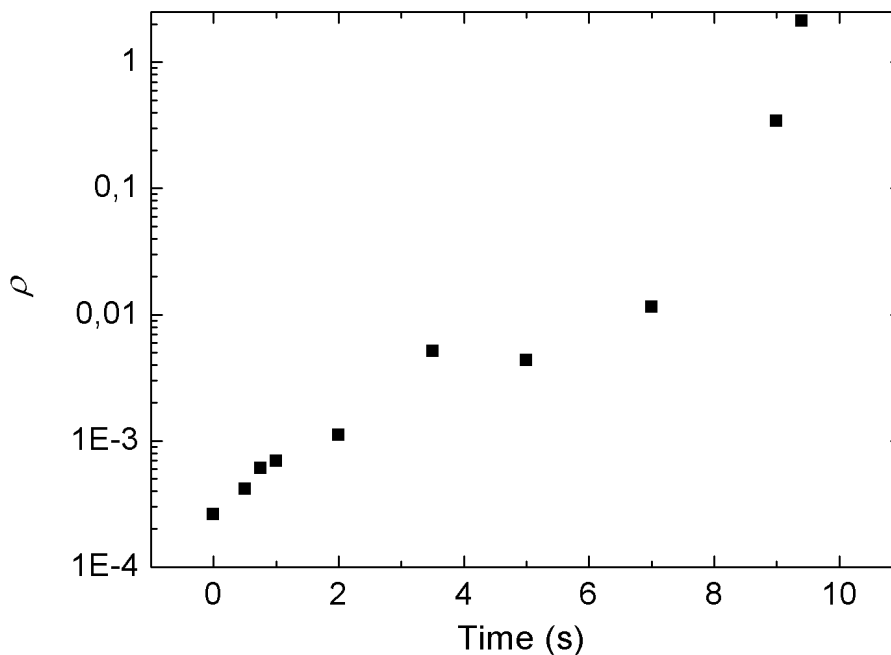


Image 15: phase space density  $\rho$  measurements during the evaporative cooling process

Analyzing the absorption images of the free expanding cloud, one can first observe that it appears evidence during the evaporation towards the BEC, that lowering the temperature, gradually emerges a condensed fraction of the cloud at the center of the thermal cloud. This appears as a mixing of two different density profiles for the atoms. Those in the center of the cloud are below the critical condensation temperature ( $T_C$ ). In Image 16 we see they are well

fitted by a parabolic function, that is typical of a condensed phase (21). The remaining non-condensed fraction is instead well fitted by a Gaussian function:

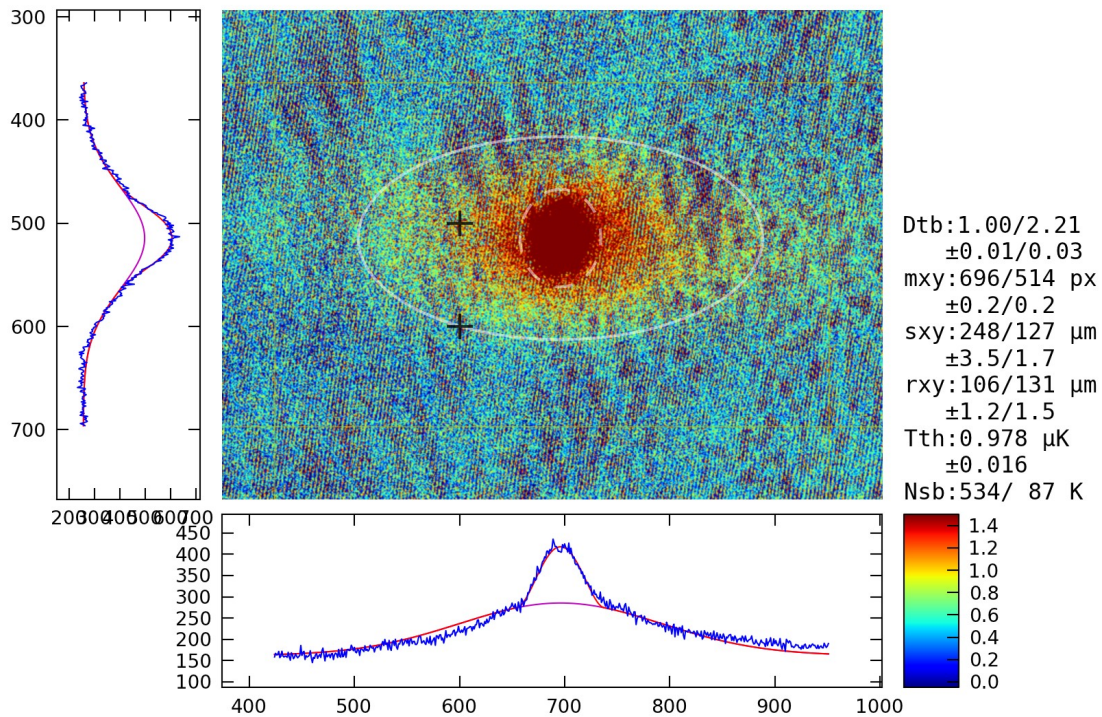


Image 16: absorption image of the potassium cloud with both condensed phase and thermal phase mixed together. The parabolic fit is reported with a mean section radius marked as “rxy” and the Gaussian fit that is typical of a thermal cloud with a mean square root of variance marked as “sxy”

One can now collect a plenty of these measurements and plot the corresponding fraction of the atoms in the condensed phase versus the temperature, which is possible to compute with a Maxwell-Boltzmann velocities distribution from the thermal fraction of the cloud that is in a free expansion regime, taking in account the time past since the release of the cloud and the triggering of the CCD camera.

We expect the functional relation of the condensed fraction against the measured temperature to be [13]:

$$(55) \quad N(T) = N_0 \left[ 1 - \left( \frac{T}{T_c} \right)^3 \right].$$

I did use this to fit the data and to compute  $T_c = (616 \pm 7) \text{nK}$  (Image 17).

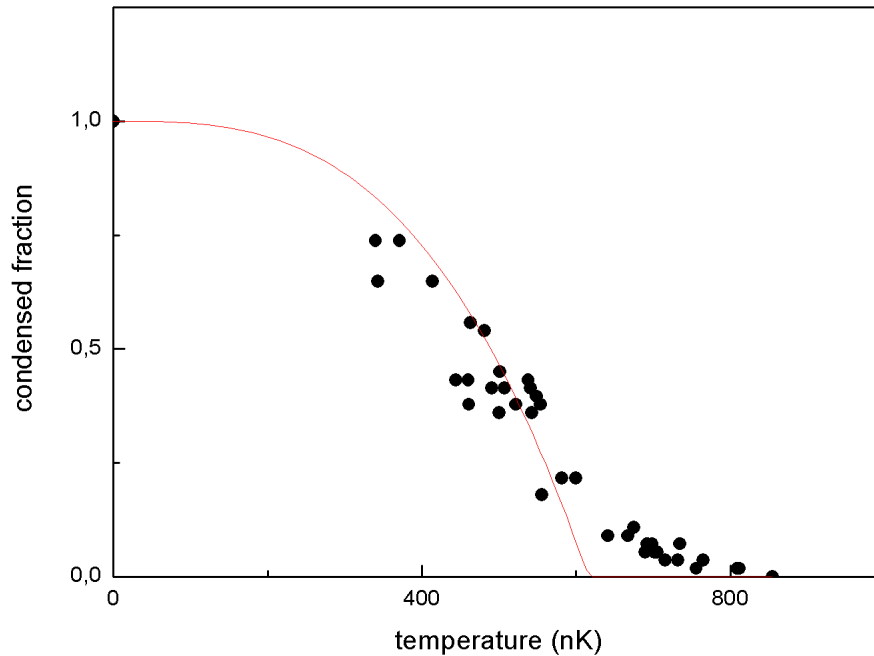


Image 17: the fraction of atoms in the condensed phase at temperatures close to the critical transition temperature  $T_c$

This is quite similar to the theoretical value, that can be computed as [13] :

$$(56) \quad k T_c \approx 0.94 \hbar \omega_{ho} \sqrt[3]{N}$$

for a cloud with  $N = 5 \times 10^5$ ,  $\omega_{ho} = 2\pi \times 200 \text{Hz}$  :

$$(57) \quad T_c = 716 \text{ nK} .$$

The critical temperature computed using equation (55) doesn't actually fit perfectly. This is due to the dependence from the number of trapped atoms, that is clear looking at equation (56). As we can see  $T_c \propto \sqrt[3]{N}$ , so that  $T_c$  is large at the start of the evaporation ramp and decreases while the evaporation proceeds towards the pure condensate. the fitting curve should then evolve as shown in Image 18.

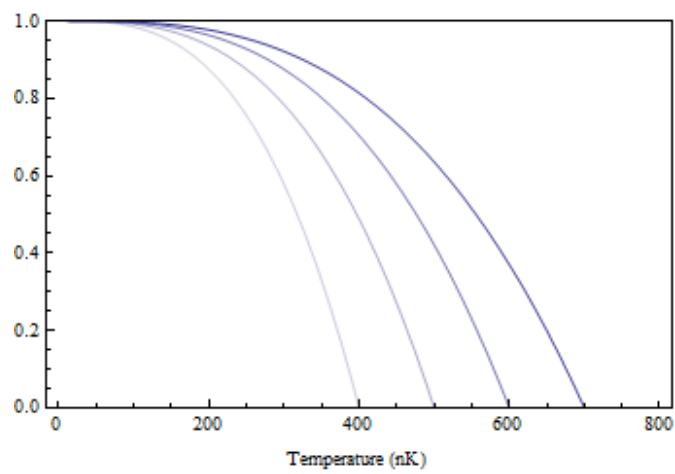


Image 18: shows the lowering effect on the critical temperature due to loss of atoms during the evaporation

This explains why the fitted  $T_c$  is smaller than the theoretical expectation and why the measures gradually get under the plotted curve.

## 4.7 Interaction control

Feshbach resonances offer great possibilities for tuning the interaction in ultracold atomic clouds. As we can find in [14] at  $B_0=402.4$  G, the  $|1,1\rangle$  state of  $^{39}\text{K}$  has a Feshbach resonance with  $\Delta=52$  G, this is quite convenient experimentally for tuning the two-body scattering length.

The next figure shows clear evidence of the Feshbach resonance in  $|1,1\rangle$ , it reports the absorption images taken on the cloud, in free expansion after releasing the trap, for various scattering lengths

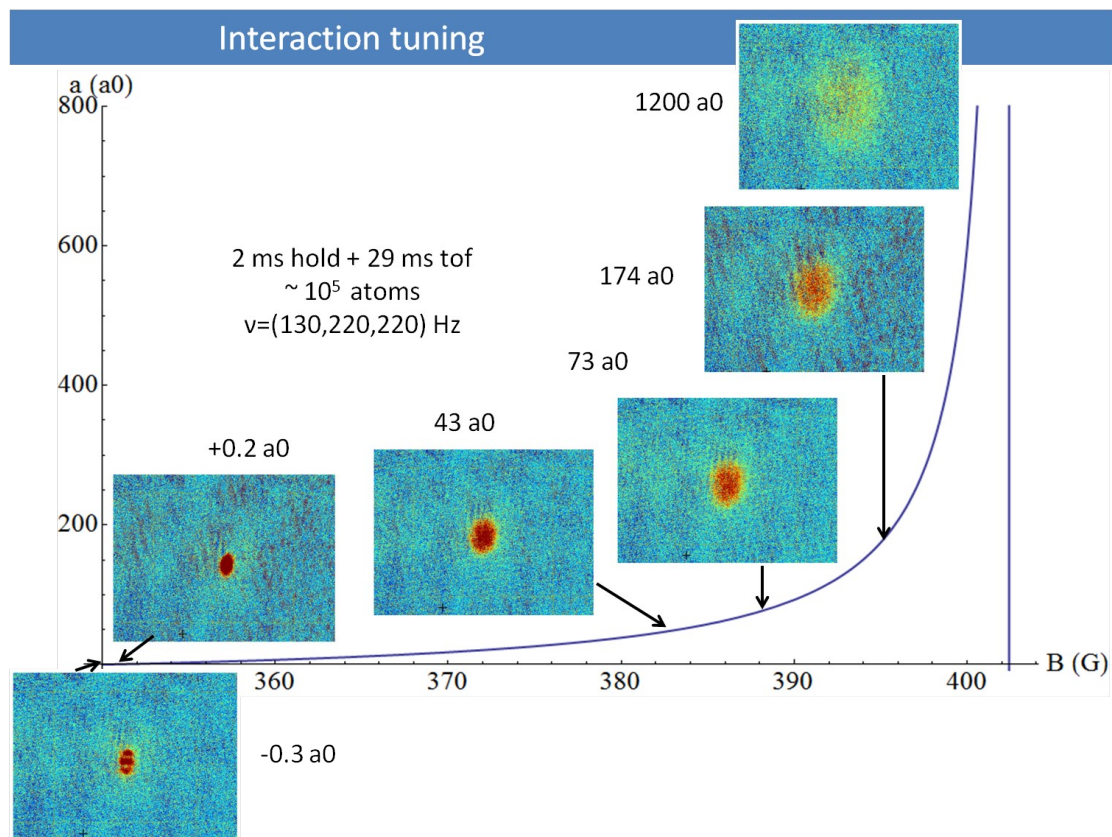


Image 19: the Feshbach resonance that shows the 2-body scattering length corresponding to different values of magnetic field generated by the Feshbach coils

in proximity of the Feshbach resonance the scattering length is found to follow the parametric relation

$$(58) \quad a(B) = a_{bg} \left( 1 - \frac{\Delta}{B - B_0} \right) .$$

One can note how the size of the cloud in expansion increases as the interaction is increased along the Feshbach resonance, in agreement with the expectations.

Let us now discuss more quantitatively the evolution of the cloud size. First of all, one must make a distinction between the region close to the zero-crossing, where the sample is practically non-interacting, and the remaining regions of moderate and large interactions. In the first case the kinetic energy of the trap will dominate over the interaction energy, while in the second case the kinetic energy is negligible (Thomas-Fermi approximation) and the interaction energy alone will drive the expansion.

In the non interacting case the dimension of the expanding cloud depends only on the dimensions of the fundamental level of the trap potential  $a_{ho} = \sqrt{\frac{\hbar}{m \omega_{ho}}}$ . In fact, before releasing the trap potential one assumes to be in an equilibrium condition, the energy of the fundamental level in the harmonic potential is  $\frac{\hbar \omega_{ho}}{2}$  and for the equipartition principle we have

$$(59) \quad E = E_{kin} + E_{pot} = \frac{\hbar \omega_{ho}}{4} + \frac{\hbar \omega_{ho}}{4} = \frac{1}{2} m \omega_{ho}^2 \langle x^2 \rangle + \frac{1}{2} m \langle v^2 \rangle .$$

The wave function has a Gaussian profile and the square root of the variance represents

the dimensions of the atomic cloud in the fundamental state  $\sigma_0 = \frac{a_{ho}}{\sqrt{2}}$ <sup>1</sup>, and it is the initial dimensions of the expanding cloud.

In ballistic expansion the cloud will expand with [13]

$$(60) \quad \sigma(t) = \sqrt{\sigma_0^2 + \langle v^2 \rangle t^2} = \sigma_0 \sqrt{1 + \omega_{ho}^2 t^2}$$

where  $\langle v^2 \rangle = \omega_{ho}^2 \sigma_0^2$ .

In particular for long expansion times ( which means when  $t \gg \frac{1}{\omega_{ho}}$  ) will be valid to consider the approximation

$$(61) \quad \sigma^2(t) = \sigma_0^2 (1 + \omega_{ho}^2 t^2) \sim \sigma_0^2 \omega_{ho}^2 t^2 .$$

In the interacting case, when  $E_{int} \gg \frac{\hbar \omega_{ho}}{2}$ , for long expansion times the kinetic energy is negligible and the Thomas-Fermi approximation is valid. The distribution function is then a parabola with radius [13]

$$(62) \quad R^2(t) = R^2(0) \times \frac{2}{3} \omega_{ho}^2 t^2 = \frac{2}{3} \frac{\mu}{m} t^2 \quad , t \gg \frac{1}{\omega_{ho}}$$

$$(63) \quad \Rightarrow R(t) = \sqrt{\frac{2}{3}} R(0) \omega_{ho} t$$

the 2/3 factor is due to the ratio of  $\frac{E_{int}}{E_{kin}}$ , as reported in [17].

---

1 From (59) one finds:  $\sigma_0^2 = \langle x^2 \rangle = \frac{\hbar \omega_{ho}}{4} \cdot \frac{2}{m \omega_{ho}^2} = \frac{a_{ho}^2}{2}$

In the graph below are reported the measurements (black) of the expanding cloud

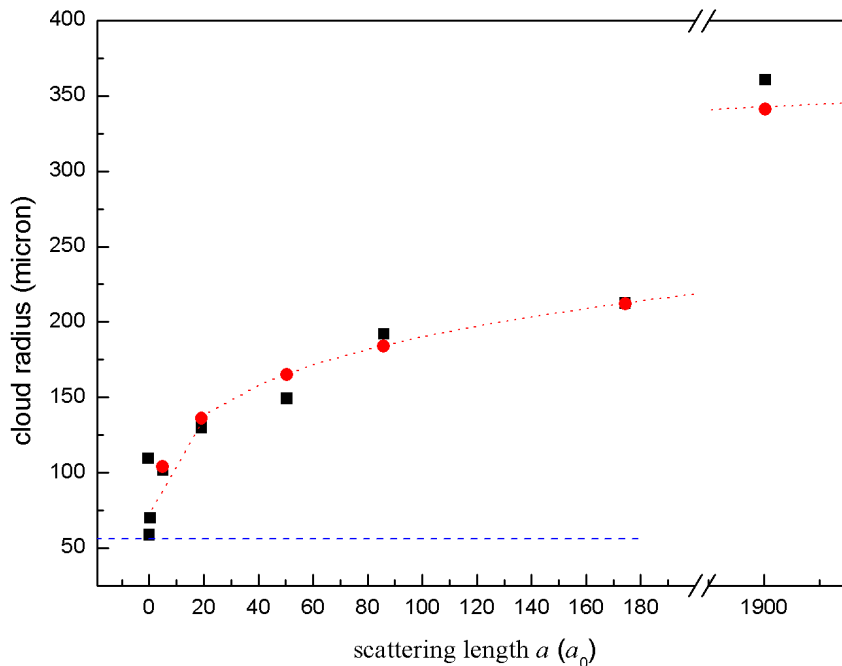


Image 20: cloud radius after a free expansion of 29 ms. The measured radii (black squares) and the calculated ones (red squares) are in quite good agreement.

The red dashed line is the Thomas-Fermi model model, while the blue dashed is the expected width of the trap's fundamental level (twice the gaussian width), which is the appropriate expectation for the expansion of weakly interacting samples.

These values are very similar to the theoretical prediction reported in red. The data reported about the zero scattering length are those for which the Thomas-Fermi limit is not valid as interactions are highly suppressed. The blue line sets the value of the dimension of the fundamental level in the trap. This is the low limit of the expanding cloud as the scattering length is lowered to zero.

It comes out in the Thomas-Fermi limit a very high dependence between expansion of the cloud and the scattering length  $a$ , in fact considering (24) and (62) one finds

$$(64) \quad R \propto a^{\frac{1}{5}}$$

Let us now comment on the expansion of a system with slightly negative scattering length ( $a = -0.3 a_0$ , leftmost picture in Image 19). It is well known that a trapped condensate cannot be stable in presence of an attractive interaction that is not counterbalanced by the kinetic energy of the ground state of the trap. As a matter of fact, a BEC in our trap is expected to become unstable as soon as the scattering length becomes negative by a fraction of a Bohr radius. The instability results in a fast acceleration of portions of the cloud and possibly in the formation of solitons. This might be the case of the condensate in Image 21, where one can clearly see a cloud that is split into different components

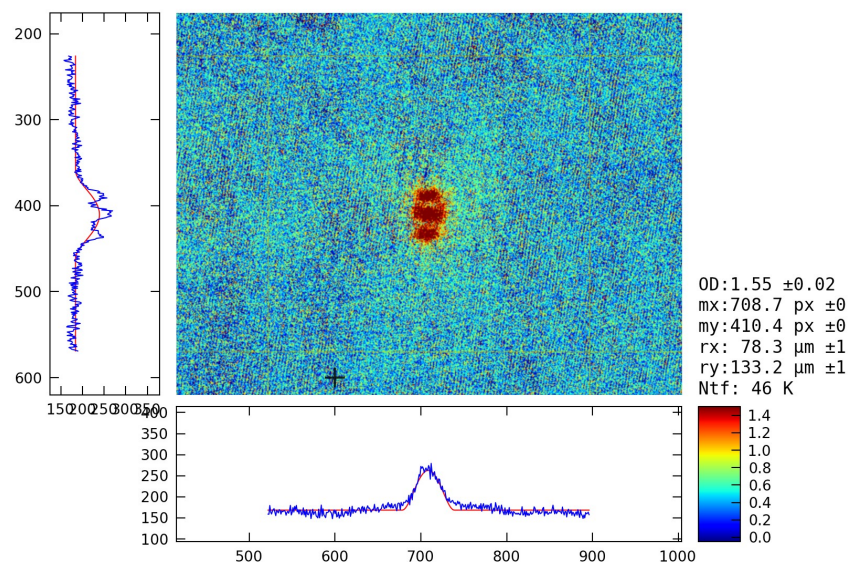


Image 21: absorption image of the cloud after a free expansion with attractive interactions ( $a = -0.3 a_0$ )

To finish, these measurements demonstrate the possibility of tuning to a large extent the interaction energy in a  $^{39}\text{K}$  Bose-Einstein condensate. Note indeed how the system we explored ranges from essentially the ground state of the trap to an interacting system with a measured expansion velocity about seven times larger, with an energy that is then about 50 times larger than the first one.



# 5 Conclusions

In this thesis I have described the realization of a complex apparatus to prepare ultracold samples of  $^{39}\text{K}$ , an atom with exceptional tuning properties that will allow a variety of advanced experiments on macroscopic quantum systems. In particular, I have described the complex sequence of delicate phases of laser cooling, magnetic and optical trapping, and evaporative cooling that are necessary to prepare Bose-Einstein condensates of this atomic species. This was the first time that  $^{39}\text{K}$  was cooled to quantum degeneracy without the help of a second atomic species, and various stages of cooling, including sub-Doppler laser cooling and Feshbach-assisted evaporation, had to be properly designed and optimized. Once demonstrated the realization of stable Bose-Einstein condensates, I have also described a first experiment on the tuning of the two-body interaction via a Feshbach resonance. A study of the expansion of the sample from the trap has indeed shown a large variation of the interaction energy within the condensate, in accordance with theoretical expectations.

This system is now ready to perform a novel class of experiments on quantum gases with tunable interaction. One important example is an exploration of the fundamental limits of quantum interferometry with atoms. A question that would be important to solve is the following: is it possible to perform interferometry with sensitivity approaching the Heisenberg limit, by employing matter waves? The tuning of the interaction would indeed allow to use it to create entanglement at the interferometer's input, and later cancel it to operate the interferometer in the linear regime.

Another important question is related for example to a clarification of universal phenomena

in the Efimov effect, i.e. the appearance of a ladder of weakly bound three-particles bound states at a two-body resonance. More and more advantages from having a Bose-Einstein condensate with tunable interaction appear also in the field of disordered systems, where the interplay of disorder and interactions is in the focus of various fields of physics.

During this work I realized to have acquired in University of Florence, the knowledge needed to work all the complicated experimental apparatus that the laboratory requires and the theory needed to understand and describe it.

From theory to practice.





- 1: M. H. Anderson, J. R. Ensher, M. R. Matthews, C. E. Wieman, E. A. Cornell "Observation of a Bose-Einstein condensate in a dilute atomic vapor" *Science* - 1995
- 2: M. B. Dahan, E. Peik, J. Reichel, Y. Castin and C. Salomon, "Bloch Oscillations of Atoms in an Optical Potential" *Phys. Rev. Lett.* 76, 45084511 - 1996
- 3: Markus Greiner, Olaf Mandel, Tilman Esslinger, Theodor W. Haensch and Immanuel Bloch "Quantum phase transition from a superfluid to a Mott insulator in a gas of ultracold atoms" *Nature* - 2002
- 4: G. Roati, C. D'Errico, L. Fallani, M. Fattori, C. Fort, M. Zaccanti, G. Modugno, M. Modugno and M. Inguscio "Anderson localization of a non-interacting condensate" *Nature* - 2008
- 5: T.W. Haensch and A. L. Schawlow "Cooling of gases by laser radiation" *Optics Communications* - 1975
- 6: D. J. Wineland, J. Dalibard and C. Cohen-Tannoudji "Sisyphus cooling of a bound atom" *JOSA B* - 1992
- 7: G. Modugno, G. Ferrari, G. Roati, R. J. Brecha, A. Simoni and M. Inguscio "Bose-Einstein condensation of potassium atoms by sympathetic cooling" *Science* - 2001
- 8: G. Roati, M. Zaccanti, C. D'Errico, J. Catani, M. Modugno, A. Simoni, M. Inguscio and G. Modugno "39K Bose-Einstein condensate with tunable interactions" *Phys. Rev. Lett.* 99 - 2007
- 9: G. Roati, F. Riboli, G. Modugno and M. Inguscio "Fermi-Bose Quantum Degenerate 40K-87Rb Mixture with Attractive Interaction" *Phys. Rev. Lett.* - 2002
- 10: T. Kishimoto, J. Kobayashi, K. Noda, K. Aikawa, M. Ueda and S. Inouye "Direct evaporative cooling of 41K into a Bose-Einstein condensate" *Phys. Rev. Lett.* - 2002
- 11: K. Dieckmann, R. J. C. Spreeuw, M. Weidemüller and J. T. M. Walraven "Two-dimensional magneto-optical trap as a source of slow atoms" *Phys. Rev. A* - 1998
- 12: E. L. Raab, M. Prentiss, Alex Cable, Steven Chu and D. E. Pritchard "Trapping of Neutral Sodium Atoms with Radiation Pressure" *Phys. Rev. Lett.* - 1987
- 13: Pethick, C., H. Smith, Bose-Einstein Condensation in Dilute Gases,, 213-214,, 2008
- 15: C. Chin, R. Grimm, P. Julienne, E. Tiesinga "Feshbach resonances in ultracold gases" *Rev. Mod. Phys.* 82 1225-1286 - 2010
- 16: G.M. Tino, *Fisica Atomica*,,,,,, 2006
- 18: Franco Nori "Superconducting qubits: Atomic physics with a circuit" *Nature Physics* 4 - 2008
- 14: C. D'Errico, M. Zaccanti, M. Fattori, G. Roati, M. Inguscio, G. Modugno, and A. Simoni "Feshbach resonances in ultracold 39K" *New J. Phys.* 9 223 - 2007
- 17: Dalfovo et al. "Bose Einstein condensation in trapped gases" *Rev. Mod. Phys.* 3 479 - 1999